Department of Chemistry

Synthesis and Characterization of Ternary Manganese Oxides

Kristina Uusi-Esko

Aalto University

DOCTORAL DISSERTATIONS

Aalto University publication series
DOCTORAL DISSERTATIONS 56/2011

Synthesis and Characterization of Ternary Manganese Oxides

Kristina Uusi-Esko

Doctoral dissertation for the degree of Doctor of Science in Technology to be presented with due permission of the School of Chemical Technology for public examination and debate in Auditorium KE2 (Komppa Auditorium) at the Aalto University School of Chemical Technology (Espoo, Finland) on the 19th of August 2011 at 12 noon.

Aalto University
School of Chemical Technology
Department of Chemistry
Laboratory of Inorganic Chemistry

Supervisor
Academy Professor Maarit Karppinen

Preliminary examiners
Professor Tapani Pakkanen, University of Eastern Finland, Finland
Professor Kornelius Nielsch, University of Hamburg, Germany

Opponent
Professor Ola Nilsen, University of Oslo, Norway

Aalto University publication series
DOCTORAL DISSERTATIONS 56/2011

ISBN 978-952-60-4178-0 (pdf)
ISBN 978-952-60-4177-3 (printed)
ISSN-L 1799-4934
ISSN 1799-4942 (pdf)
ISSN 1799-4934 (printed)

Aalto Print
Helsinki 2011

Finland

The dissertation can be read at http://lib.tkk.fi/Diss/

Aalto University

Abstract

Aalto University, P.O. Box 11000, FI-00076 Aalto www.aalto.fi

Author
Kristina Uusi-Esko

Name of the doctoral dissertation
Synthesis and Characterization of Ternary Manganese Oxides

Publisher School of Chemical Technology

Unit Department of Chemistry

Series Aalto University publication series DOCTORAL DISSERTATIONS 56/2011

Field of research Inorganic Chemistry

Manuscript submitted 4 May 2011 **Manuscript revised**

Date of the defence 19 August 2011 **Language** English

☐ **Monograph** ☒ **Article dissertation (summary + original articles)**

Abstract

The demand for novel functional materials is a never-ending challenge, as the development of many future applications depends on the new innovations made in the field of materials science. Ternary manganese oxides are a versatile group of materials with interesting magnetic properties and several potential applications, e.g. in microelectronics and solid oxide fuel cells. This thesis reports the preparation of several ternary manganese oxide materials through a selection of synthesis methods. Studies on the structural details, magnetic properties and oxygen stoichiometry of the bulk and thin-film samples are moreover included in this work. The thesis consists of four publications, discussed with relevant literature data.

The synthesis of an entire series of the hexagonal $R\mathrm{MnO_3}$ system for R = Y, Ho-Lu, and the subsequent conversion of the hexagonal phases to orthorhombic perovskites through high-pressure treatment is realized in the present work. The synthesis methods of the hexagonal bulk samples reported here include the hydrothermal and the sol-gel methods. A systematic study of the structural evolution is presented for both polymorphs, and studies on the magnetic properties have been performed as well. High-quality thin-film samples of the hexagonal and orthorhombic $R\mathrm{MnO_3}$ families have been fabricated employing the atomic layer deposition (ALD) technique and post-deposition heat treatment. The formation of metastable orthorhombic $R\mathrm{MnO_3}$ perovskites of the small rare earths has been successfully realized even for the smallest R constituent, Lu, by depositions on coherent perovskite substrates with low lattice mismatch with the targeted structure. The challenging task of studying the magnetic properties of these thin-film samples is also approached in the present work. The Néel temperatures determined for the $R\mathrm{MnO_3}$ films featuring antiferromagnetic ordering are in good accordance with the corresponding results on powder samples, and the presence of cation vacancies is shown for the ALD-grown $\mathrm{LaMnO_{3+\delta}}$ sample.

The reproducible fabrication of spinel-structured $\mathrm{(Mn,Co)_3O_4}$ thin films by ALD has been achieved and reported. Precise control of the oxygen content of as-deposited $\mathrm{MnCo_2O_{4+\delta}}$ films has been realized for the first time for an ALD-grown thin-film sample through post-deposition heat treatments, as evidenced from the monotonous increases of both the unit-cell volume and the Curie temperature with increasing annealing temperature/decreasing oxygen partial pressure. The performance of ALD-grown $\mathrm{MnCo_2O_4}$ protective coatings is also reported on ferritic stainless steel in solid oxide fuel cells with promising results.

Keywords manganese oxide, high-pressure synthesis, atomic layer deposition, thin film, magnetic properties, oxygen stoichiometry

ISBN (printed) 978-952-60-4177-3 **ISBN (pdf)** 978-952-60-4178-0

ISSN-L 1799-4934 **ISSN (printed)** 1799-4934 **ISSN (pdf)** 1799-4942

Location of publisher Espoo **Location of printing** Helsinki **Year** 2011

Pages 88 **The dissertation can be read at** http://lib.tkk.fi/Diss/

A? Aalto-yliopisto

Tiivistelmä

Aalto-yliopisto, PL 11000, 00076 Aalto www.aalto.fi

Tekijä
Kristina Uusi-Esko

Väitöskirjan nimi
Ternääristen mangaanioksidien synteesi ja karakterisointi

Julkaisija Kemian tekniikan korkeakoulu

Yksikkö Kemian laitos

Sarja Aalto University publication series DOCTORAL DISSERTATIONS 56/2011

Tutkimusala Epäorgaaninen kemia

Käsikirjoituksen pvm 04.05.2011 **Korjatun käsikirjoituksen pvm**

Väitöspäivä 19.08.2011 **Kieli** Englanti

☐ **Monografia** ☒ **Yhdistelmäväitöskirja (yhteenveto-osa + erillisartikkelit)**

Tiivistelmä

Tulevaisuuden sovelluskohteet vaativat jatkuvaa työtä uusien funktionaalisten materiaalin kehittämiseksi. Ternääriset mangaanioksidit muodostavat monipuolisen joukon materiaaleja, joilla on mielenkiintoisia magneettisia ominaisuuksia sekä monia potentiaalisia sovelluskohteita, esim. mikroelektroniikassa ja kiinteäoksidipolttokennoissa. Tässä väitöskirjassa esitetään useiden ternääristen mangaanioksidimateriaalien valmistus erilaisia synteesimenetelmiä käyttäen.

Tässä väitöskirjatutkimuksessa toteutettiin ensin heksagonaalisen $R\mathrm{MnO_3}$-sarjan (R = Y, Ho-Lu) synteesi, jonka jälkeen heksagonaaliset faasit puristettiin korkeassa paineessa ortorombisiksi perovskiiteiksi. Heksagonaalisten pulverinäytteiden synteesimenetelminä käytettiin sooli-geelimenetelmää sekä hydrotermistä tekniikkaa. Molempien kidemuotojen rakenteellista evoluutiota sekä magneettisia ominaisuuksia tutkittiin systemaattisesti harvinaisen maametallin koon funktiona.

Sekä heksagonaalisen että ortorombisen $R\mathrm{MnO_3}$-sarjan materiaaleja valmistettiin korkealaatuisina ohutkalvoina käyttäen atomikerroskasvatusta (atomic layer deposition, ALD) sekä kasvatuksen jälkeistä lämpökäsittelyä. Metastabiilien ortorombisten $R\mathrm{MnO_3}$-perovskiittien (R = Y, Yb, Lu) valmistus onnistuttiin toteuttamaan kasvattamalla kalvot perovskiittisubstraateille, joiden kiderakenne poikkeaa vain vähän tavoitteena olevasta kiderakenteesta. Lisäksi tässä väitöskirjassa tutkittiin ohutkalvojen magneettisia ominaisuuksia, joiden mittaaminen on pienestä näytemäärästä johtuen usein haastavaa. Antiferromagneettisesti järjestäytyvien $R\mathrm{MnO_3}$-kalvojen Néelin lämpötilojen havaittiin olevan hyvin samankaltaisia pulverinäytteiden vastaavien muutoslämpötilojen kanssa. Magneettisten ominaisuuksien avulla voitiin myös osoittaa kationivakanssien läsnäolo $\mathrm{LaMnO_{3+\delta}}$-ohutkalvonäytteissä.

Spinellirakenteisia $(\mathrm{Mn,Co})_3\mathrm{O_4}$-ohutkalvoja kasvatettiin tässä työssä toistettavasti ALD-menetelmällä. Atomikerroskasvatuksella valmistetun kalvon happistoikiometrian säätelyssä onnistuttiin ensimmäistä kertaa $\mathrm{MnCo_2O_{4+\delta}}$-kalvojen tapauksessa. Kalvonäytteiden happipitoisuutta voitiin kontrolloida eri lämpötiloissa tehtävillä lämpökäsittelyillä ja happipitoisuuden muuttuminen voitiin havaita sekä yksikkökopin tilavuuden että Curien lämpötilan kasvuna käsittelylämpötilan kasvaessa/hapen osapaineen laskiessa. Tässä väitöskirjassa tutkittiin myös ALD-menetelmällä kasvatettujen $\mathrm{MnCo_2O_4}$-korroosionestopinnoitteiden suorituskykyä kiinteäoksidipolttokennojen teräsosien suojaamisessa.

Avainsanat mangaanioksidi, korkeapainesynteesi, atomikerroskasvatus, ohutkalvo, magneettiset ominaisuudet, happistoikiometria

ISBN (painettu) 978-952-60-4177-3 **ISBN (pdf)** 978-952-60-4178-0

ISSN-L 1799-4934 **ISSN (painettu)** 1799-4934 **ISSN (pdf)** 1799-4942

Julkaisupaikka Espoo **Painopaikka** Helsinki **Vuosi** 2011

Sivumäärä 88 **Luettavissa verkossa osoitteessa** http://lib.tkk.fi/Diss/

PREFACE

The work presented in this thesis was carried out in the Laboratory of Inorganic Chemistry at Aalto University School of Chemical Technology and Materials and Structures Laboratory, Tokyo Institute of Technology, between March 2007 and April 2011. Academy of Finland (Nos 114517, 116254 and 126528), Materials and Structures Laboratory (Tokyo Tech), Finnish Foundation for Technology Promotion and The Emil Aaltonen Foundation are gratefully acknowledged for the financial support of this work.

I want to thank my supervisor and instructor Academy Professor Maarit Karppinen for the opportunity for postgraduate studies and the constant encouragement. It has been fascinating to work within materials chemistry and atomic layer deposition under such inspiring supervision. I would also like to thank Professor Hisao Yamauchi for letting me stay with his group in Japan, and Dr. Naoki Imamura for his help with the HP experiments. Special thanks belong to Mr. Jari Malm and Dr. Pia Myllymäki for introducing me to the world of atomic layer deposition. From the bottom of my heart, I also want to thank Dr. Eeva-Leena Rautama for her endless patience and all her guidance and support concerning Rietveld refinement, SQUID measurements and life in general. Furthermore, I want to thank Dr. Timo Sajavaara and Mr. Mikko Laitinen for sharing their expertise in RBS, and all my co-workers at the Laboratory of Inorganic Chemistry and Materials and Structures Laboratory for their help with the practicalities and for all their support.

Most importantly, I want to thank my incredibly supporting family, Eija, Teemu, Juha, Erkki, my awesome sister Katarina and the ones no longer with us, for always being there for me. My warmest thanks belong to the Raunio family for all the help and encouragement. I also want to thank all my friends and two very important little girls, Nelly and Emilia, for the happiness you bring into my life. And finally, thank you Tapani for supporting and loving me through it all.

Kristina Uusi-Esko

Espoo, May 2011

CONTENTS

LIST OF PUBLICATIONS

In addition to the present review, this thesis includes the following publications (**I-IV**), which are referred to in the text by their corresponding Roman numbers. The original publications are found in appendices **I-IV**.

I K. Uusi-Esko, J. Malm, N. Imamura, H. Yamauchi, M. Karppinen, Characterization of RMnO$_3$ (R = Sc, Y, Dy-Lu): High-Pressure Synthesized Metastable Perovskites and Their Hexagonal Precursor Phases, *Mater. Chem. Phys.* **112** (2008) 1029-1034.

II K. Uusi-Esko, J. Malm, M. Karppinen, Atomic Layer Deposition of Hexagonal and Orthorhombic YMnO$_3$ Thin Films, *Chem. Mater.* **21** (2009) 5691-5694.

III K. Uusi-Esko, E.-L. Rautama, M. Laitinen, T. Sajavaara, M. Karppinen, Control of Oxygen Nonstoichiometry and Magnetic Property of MnCo$_2$O$_4$ Thin Films Grown by Atomic Layer Deposition, *Chem. Mater.* **22** (2010) 6297-6300.

IV K. Uusi-Esko, M. Karppinen, Extensive Series of Hexagonal and Orthorhombic RMnO$_3$ (R = Y, La, Sm, Tb, Yb, Lu) Thin Films by Atomic Layer Deposition, *Chem. Mater.* **23** (2011) 1835-1840.

THE AUTHOR'S CONTRIBUTION

Publication I — The author defined the research plan together with co-authors, synthesized the samples and performed all the characterizations. The results were interpreted together with co-authors. The author had a major role in writing the manuscript.

Publication II — The author defined the research plan together with co-authors and carried out the experimental work. The results were interpreted together with the co-authors. The author had a major role in writing the manuscript.

Publication III — The author defined the research plan together with co-authors, performed the film depositions and the characterizations excluding the RBS measurements. The author had a major role in writing the manuscript.

Publication IV — The author defined the research plan together with the co-author, carried out the experimental work and had a major role in writing the manuscript.

Espoo 4th of May 2011

Acad. Prof. Maarit Karppinen

LIST OF ABBREVIATIONS AND SYMBOLS

AFM	Antiferromagnetic
ALD	Atomic layer deposition
ASR	Area specific resistance
CMR	Colossal magnetoresistance
CN	Coordination number
EDTA	Ethylenediaminetetraacetic acid
FC	Field cooling
FM	Ferromagnetic
GPC	Growth per cycle
HP	High pressure
JT	Jahn-Teller
RBS	Rutherford backscattering spectrometry
SOFC	Solid oxide fuel cell
SQUID	Superconducting quantum interference device
thd	2,2,6,6-tetramethyl-3,5-heptanedionate
XRD	X-ray diffraction
XRF	X-ray fluorescence
ZFC	Zero-field cooling

δ	Oxygen nonstoichiometry parameter
χ	Magnetic susceptibility
μ_B	Bohr magneton
μ_{eff}	Effective paramagnetic moment
R	Rare-earth element
$r(R^{III})$	Ionic radius of a trivalent rare-earth cation
T_C	Curie temperature
T_{dep}	Deposition temperature
T_{FE}	Ferroelectric transition temperature
T_N	Néel temperature
T_{sub}	Precursor sublimation temperature
t	Goldschmidt tolerance parameter

1 INTRODUCTION

In the search for new functional materials, the use of special synthesis conditions can offer remarkable possibilities. Bending the rules set by thermodynamics under ambient conditions can be the key to solutions that would otherwise merely remain as a dream in a scientist's brain. One of the most powerful tools for realizing new materials is the high-pressure (HP) technique[1-3] which utilizes both ultra-high solid-medium pressures (2-8 GPa) and high oxygen gas pressures (10-200 atm) to enable the formation of new enticing crystal structures. Originally, the HP method was developed to produce synthetic diamonds, but later the technique turned out to be quite the 'diamond' itself. It is a technique that makes it possible to prepare not only carbon diamonds but also a variety of metastable structures of other elements and their combinations. The HP technique can be used for either the synthesis of a material or the conversion of the crystal structure, as is the case for diamonds. The special synthesis conditions of the HP method have, for example, been of excellent use in the search for copper oxide superconductors in the 1990s.[2,4,5]

After the initial discovery of a novel phase with promising properties, the need to bring the new material closer to the potential applications by producing it, *e.g.* in thin-film form, tends to become relevant. When it comes to stabilizing metastable phases, the range of techniques one can turn to is rather limited. Epitaxial phase stabilization is an option that has been used to obtain many metastable oxides in spite of their thermodynamic instability in bulk form.[6-10] Epitaxial phase stabilization is a technique in which the preparation of metastable phases as thin films is based on free-energy gain at the film/substrate interface. Although it may be far from the ideal solution for large-scale manufacturing, it can still be considered as a link between a laboratory and the potential applications of a novel functional material. Moreover, the future applications of many materials likely depend on the possibilities of large-scale production in thin-film form. Atomic layer deposition (ALD) is a technique that allows the deposition of conformal and pin-hole free films on large uneven surfaces.[11,12] It is also a technique that is already used in industrial-scale production[13] with steady progress being made in the field of continuous ALD processes. ALD is a gas-phase method which is based on alternate pulsing of the precursors separated by in-

ert-gas purging. Thus, gas-phase reactions are eliminated and the film growth proceeds exclusively through surface reactions. Due to this self-limiting growth mechanism, the resulting films are of exceptionally high quality. Moreover, both the thickness and the composition can be accurately controlled even on large substrate areas.

The deposition of ternary oxide films has long been a challenge for the ALD community. The search for compatible precursors that meet the requirements set by the technique can be a difficult task. In addition, the cation stoichiometry has to be well under control in order to achieve the desired material reproducibly. Interestingly, for years the deposition of ternary oxide materials was almost an intimidating topic. One possible explanation could be the rather persistent search for 'ALD windows', or temperature ranges of constant growth per cycle (GPC), in the early years of ALD research. It was important to find preferably wide and overlapping ALD windows for the binary oxides before depositing any ternary oxide films. Later, however, it became evident that while designing ALD processes for ternary or more complex materials, overlapping ALD windows of the constituent binary oxides can be impossible to find and are often not even needed. Today, the search for new application possibilities of the ALD method has taken the ALD community towards more and more advanced processes.[12,14] As the selection of ALD processes expands, an open mind might be the best tool for allowing further progress to happen.

Compared to the control of the cation ratio in ternary or more complex oxide materials, the control of oxygen stoichiometry is clearly a less studied problem. Alterations in oxygen stoichiometry are, however, everyday life for those studying the vast possibilities of the perovskite and related frameworks. By altering the oxygen content, new crystal structures and properties can be found to enrich the selection of functional oxide materials. Changes in oxygen stoichiometry tend to affect especially the magnetic and transport properties of materials. Thus, it is often reasonable to study these properties together with the oxygen stoichiometry of a material.

The constant demand for new functional materials with potential applications especially among data storage has led to an intensive search for new magnetically interesting structures. The present study approaches a selection of magnetic ternary man-

ganese oxides of different crystal structures. Hexagonal and orthorhombic rare-earth (*R*) manganites $RMnO_3$ are an excellent example of functional oxide materials possessing enticing magnetic properties. [15-20] The hexagonal $RMnO_3$ series has been vastly studied for their multiferroic properties described as the coexistence of both ferroelectric and antiferromagnetic polarization. The interest in the orthorhombic series is mainly based on the colossal magnetoresistance (CMR) phenomenon in which an external magnetic field can cause order of magnitude changes in electrical conductivity. The members of the $(Mn,Co)_3O_4$ spinel system, in turn, have attracted wide attention due to their unusual hysteresis and magnetization process.[21-24] Preparation of $MnCo_2O_4$ at high temperatures results in a structure of a cation-deficient spinel, but low synthesis temperatures enable an increased oxygen-to-metal ratio. The possibility to control the oxygen content is not a common feature for all spinels, but possible for some.

The aim of this work was to study ternary manganese oxides with interesting magnetic properties. The preparation methods employed for the synthesis of the hexagonal bulk samples of $RMnO_3$ included the hydrothermal technique and the sol-gel method.**I** Stabilization of metastable perovskites of the $RMnO_3$ series was realized first through high-pressure conversion**I** and later by the ALD method/epitaxial phase stabilization.**II,IV** ALD processes were developed for the fabrication of $(Mn,Co)_3O_4$ spinels and an extensive series of $RMnO_3$ (*R* = Y, Sm, Tb, Er-Lu).**II,IV** The evolution of structural and magnetic properties was studied in bulk samples of both hexagonal and metastable orthorhombic $RMnO_3$ (*R* = Y, Dy-Lu) series.**I** Control of oxygen stoichiometry in thin-film samples was studied for both the perovskite**IV** and spinel**III** type structures.

2 HEXAGONAL AND ORTHORHOMBIC *R*MnO_3 SERIES

When prepared under ambient pressure, the rare-earth manganese oxides crystallize with crystal structures depending on the size of the *R* constituent: for the larger rare earths (La-Dy), orthorhombic perovskite structure is adopted whereas for the smaller rare earths (Sc, Y, Ho-Lu) a hexagonal structure forms.[25,26] The hexagonal *h*-*R*MnO_3 series host a co-existence of both antiferromagnetic (AFM) ordering of the Mn^{III} moments and ferroelectric polarization along the *c*-axis.[18,19] The fairly uncommon situation has its origin in the noncentrosymmetric structure involving the buckling observed in the *R*-atom plane which is increased with decreasing size of the rare-earth element. The orthorhombic structure, on the other hand, compensates the decreasing size of the *R* constituent through the distortion of the oxygen sublattice leading to increasing tilts of the MnO_6 octahedra. The non-doped orthorhombic *o*-*R*MnO_3 phases are antiferromagnetic insulators, however, the preparation of stoichiometric samples can be challenging in the case of the largest members of the rare-earth series. Moreover, the stoichiometric samples are often not even desired as the exciting functional properties only emerge upon increasing the concentration of Mn^{IV} on the expense of Mn^{III}. As soon as cation vacancies are formed in the structure, the presence of Mn^{IV} gives rise to ferromagnetism (FM), improving also the electrical conductivity and enhancing the colossal magnetoresistance effect.[15-17] In addition to colossal magnetoresistance, the orthorhombic *R*MnO_3 phases are known for their catalytic properties, *e.g.* as combustion catalysts.[27-29]

2.1 Synthesis Methods

Although the hexagonal structure ($P6_3cm$)[26] is adopted by the heavier rare-earth manganites (*R* = Ho-Lu) under mild synthesis conditions, heavy rare-earth manganites can be forced to convert to a metastable orthorhombic perovskite structure through methods involving increased pressure[30-34,I] or deposition in thin-film form.[35,36,II] As the preparation of the metastable perovskites becomes gradually more difficult towards the smallest members of the rare-earth series, the crystal structure adopted by the borderline compounds, $HoMnO_3$ and $YMnO_3$, under normal synthesis

conditions is largely affected by the synthesis method used.[37-40] Rather severe conditions are required for the preparation of the metastable orthorhombic RMnO$_3$ perovskites at the smallest end of the rare-earth series, but the options for the fabrication of the hexagonal RMnO$_3$ phases are much wider through several techniques including even the traditional solid-state methods. In addition to the classic ceramic methods, the preparation methods employed include the hydrothermal and sol-gel methods where the final product is obtained *via* solutions containing the desired cations. Even though single-phase samples can be obtained through both the afore-mentioned methods, the sol-gel method seems to have some advantages over the hydrothermal method as it allows larger yields, requires less special equipment, and is often less sensitive to minor changes in synthesis conditions.

In this study, the powder samples of *h*-RMnO$_3$ were prepared through sol-gel and hydrothermal synthesis methods and the *o*-RMnO$_3$ through high-pressure synthesis.[I] The present sol-gel method is based on first dissolving the metal atoms of the starting materials and then complexing them with ethylenediaminetetraacetic acid (EDTA). As a result the starting materials form a homogenous mixture. Hence, the method allows atomic level mixing of the starting materials. Upon prolonged water evaporation the gel ignites spontaneously forming a low-density product which can be pelletized and sintered. Another widely used sol-gel technique is the citrate method, which has been successfully employed to fabricate *o*-ErMnO$_3$.[39,41] The hydrothermal synthesis method, in turn, is a technique that allows the use of slightly increased pressures. The autoclaves used are generally Teflon-lined steel vessels which can be heated up to 250-350 °C. Recent publications have shown even the possibility to prepare the entire series of metastable *o*-RMnO$_3$ perovskites through this technique.[33,34] One of the attractive features of the hydrothermal method is the possibility to use rather low temperatures. In comparison, the solid-state synthesis of hexagonal rare-earth manganites requires a high-temperature sintering at 1300 °C in order to eliminate all the binary-oxide impurities. Most importantly, it is essential to eliminate Mn_3O_4 as it complicates the magnetic susceptibility measurements. However, some studies have indicated that impurity levels in general are significantly lower while using the sol-gel methods.[33,42-44]

The hydrothermal syntheses of the present work were performed in 45-ml teflon-lined steel autoclaves from Parr Instrument Company. In a typical synthesis, 2.4 mmol $MnCl_2 \cdot 4H_2O$, 3 mmol $R(NO_3)_3$ and 0.6 mmol $KMnO_4$ were separately dissolved in a small amount of water. First the $MnCl_2 \cdot H_2O$ and $R(NO_3)_3$ solutions were mixed in the autoclave and $KMnO_4$ was added to the mixture to form a brown precipitate. In a separate beaker, 12 g of KOH was dissolved in 10 ml of H_2O and added to the solution to adjust the pH strongly alkaline. Water was added to fill the vessel 70% full and the mixture was thoroughly stirred for 30 minutes. The synthesis was performed at 240 ºC under autogenous pressure for 48 hours. The crystalline product was washed several times with distilled water and dried at 105 ºC. The hydrothermal synthesis method was found to be very sensitive to synthesis conditions with pH, duration and temperature of the synthesis being the most critical factors. A minor impurity remained in the hexagonal $R\mathrm{MnO_3}$ samples despite post-annealing treatments. This impurity is very likely to be a K-rich birnessite (KBi), K_yMnO_w (where $w = 2x + y$ and y is the K:Mn ratio and $2x$ is the mean oxidation state of Mn)[43,44], as it is often formed during a hydrothermal synthesis. Several attempts were also made to prepare metastable perovskite samples, however, these experiments were not successful.

The first method employed to prepare metastable perovskites of the heavier rare-earths was the high-pressure method in the 1960s.[30] The formation of the metastable orthorhombic phases is supported by the fact that high pressures prefer the denser perovskite phase.[39] The effective coordination numbers (CN) of Mn and R are 5 and 7 in the hexagonal structure, respectively.[26] In the case of the orthorhombically distorted perovskite structure, the effective coordination numbers are CN(Mn) = 6 and CN(R) = 8.[45] The HP synthesis conditions used for the preparation of metastable rare-earth manganites are rather severe. The applied pressure varies between 4 and 5 GPa, and the temperature is in the range of 800-1100 °C.[31,32,45] In addition to the synthesis of the metastable $R\mathrm{MnO_3}$ perovskites, the HP method enables the hole-doping of the $R\mathrm{MnO_3}$ perovskites[45] and the preparation of highly cation-deficient $LaMnO_{3+\delta}$ or $La_{1-x}Mn_{1-x}O_3$.[46] Both of these topics are rather interesting as they strive for enhancing the CMR effect. In this study, the members of the metastable *o*-$R\mathrm{MnO_3}$ series were synthesized by a two-step route in which the hexagonal oxides were pre-

pared under normal pressure using the sol-gel method, and then converted to the orthorhombic perovskite structure through HP treatment at 5 GPa and 800 °C.[I]

Thin-film methods used to prepare metastable orthorhombic rare-earth manganites include pulsed layer deposition[35] and metal-organic chemical vapor deposition[36]. The present study demonstrates for the first time the fabrication of metastable *o*-RMnO$_3$ thin films (R = Y, Yb, Lu) through ALD and subsequent heat-treatment.[I,IV] Over the past few years, epitaxial phase stabilization has been employed not only to fabricate metastable *o*-RMnO$_3$[35,36,II,IV] of the smaller Rs but also metastable *h*-RMnO$_3$ of the larger Rs (R = Dy, Gd, Sm).[47-49] The substrate crystals used to achieve the desired metastable phases include LaAlO$_3$(100)[35,36,II,IV], SrTiO$_3$(100)[35,36,II,IV] and NdGaO$_3$(110)[35] for metastable orthorhombic RMnO$_3$, and *h*-YMnO$_3$(110)[49], Pt(111)//Al$_2$O$_3$(0001)[48] and YSZ(111)[47,48] (YSZ: yttria-stabilized zirconia) for metastable hexagonal RMnO$_3$. The fabrication of metastable *h*-RMnO$_3$ with larger Rs is an interesting topic that has proven to be rather challenging. In fact, epitaxial stabilization is the only method reported thus far. Successful depositions on single-crystal substrates of *h*-YMnO$_3$(110) resulted in thin films with lattice parameters *a* increasing from 6.27 for Dy to 6.42 for Sm.[49] The slight decrease in the lattice parameter *c* observed by both Bosak *et al.*[47] and Balasubramanian *et al.*[49] was explained by significant strain in the films.

2.2 Crystal Structures

The hexagonal structure of the smaller Rs can be described as layers of Mn-centered trigonal bipyramids of MnO$_5$ that are separated by a layer of trivalent R cations (Figure 1).[26,50] In the hexagonal *h*-RMnO$_3$ system, trimerization of the Mn^{III} ions leads to displacements of various atoms: the tilting of the MnO$_5$ polyhedra and the buckling of the R-atom plane. The structure is noncentrosymmetric, because the MnO$_5$ bipyramids are tilted and shifted relative to the R^{III} ions. This is the reason for the ferroelectric polarization observed along the *c* axis in *h*-RMnO$_3$. The *h*-RMnO$_3$ compounds are also magnetic with an antiferromagnetic ordering of the Mn^{III} moments.[32] The ferroelectric transition occurs at high temperatures and the antiferro-

magnetic transition of the Mn^{III} moments at low temperatures. These two types of ordering coexist at low temperatures and thus the *h*-$RMnO_3$ compounds are multiferroic.

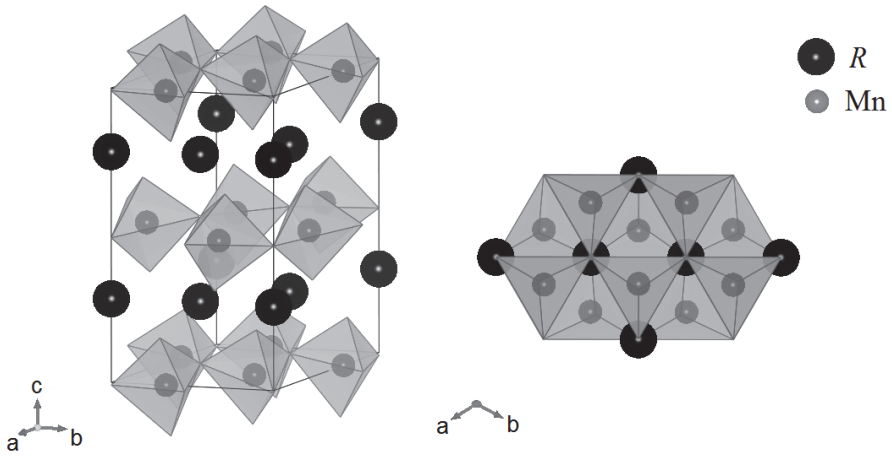

Figure 1. Polyhedral representation of the crystal structure of hexagonal *h*-$RMnO_3$. The larger spheres indicate the R^{III} ions and the smaller spheres near the center of the polyhedra indicate the Mn^{III} ions. The O^{-II} anions are located at the apexes of the polyhedra. Axial directions are marked on the left side of the figures.

The lattice parameters of the hexagonal $RMnO_3$ phases decrease monotonically as the size of the constituent rare earth decreases. The lattice parameters for samples prepared by the two powder (hydrothermal and sol-gel) methods used in the present work are shown in Figure 2. The buckling of the *R* plane is shown by the difference of the *z* position of two inequivalent *R* sites, $\Delta z \equiv z_{R1}\text{-}z_{R2}$.[I] As can be seen in Figure 3, the buckling is enhanced with decreasing ionic radius, $r(R^{III})$.

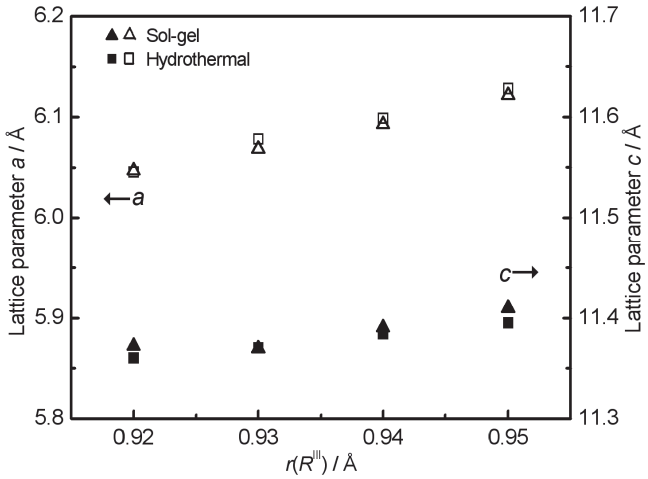

Figure 2. Lattice parameters, a and c, plotted against the ionic radius, $r(R^{III})$, for hexagonal ($P6_3cm$) RMnO$_3$ samples (R = Er-Lu) prepared through the hydrothermal and sol-gel methods.[I] The ionic radii are for the 7-coordinated R^{III} ions.[51,52]

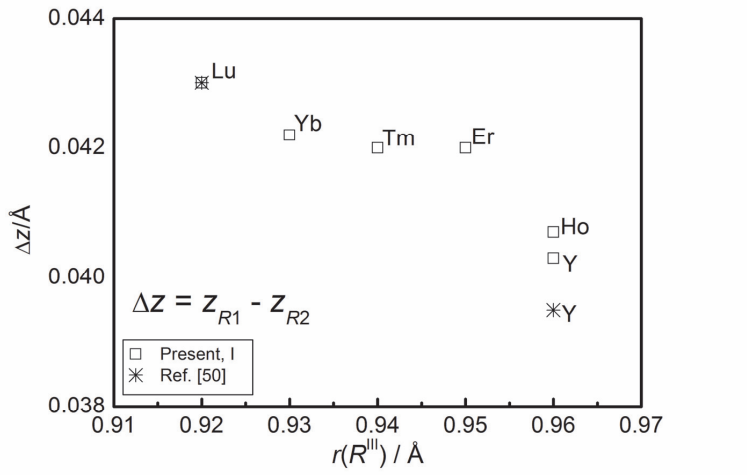

Figure 3. Decrease in the magnitude of buckling of the R plane ($\Delta z = z_{R1} - z_{R2}$) in h-RMnO$_3$ (R = Y, Ho-Lu) with the ionic radius, $r(R^{III})$.[I]

Differences between the two powder methods do not seem very significant, however a more careful observation of the X-ray diffraction patterns (shown in Figure 4) reveals that there is some anisotropic *hkl*-dependent peak broadening present in the hydrothermally synthesized samples. The 00l (l = 2n) reflections are significantly

broader with FWHM = 0.24(1)°, whereas all the other reflections have FWHM of 0.16(1)°. This could indicate that the [001] direction is affected by the platelet-like shape of the crystallites, as visualized in the SEM images. In fact, the peak width increases along the decreasing radius of R^{III} but the width of the 00*l* reflections is always one third broader compared to the rest of the pattern. In the sol-gel samples, no meaningful difference was observed within the Bragg reflections as the fitted FWHM values varied between 0.13(1)° and 0.15(1)° throughout the XRD pattern.

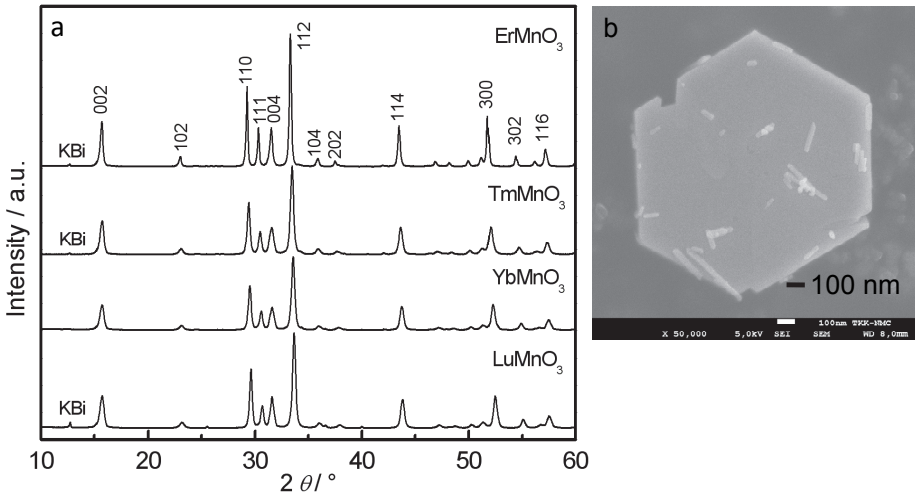

Figure 4. (a) XRD patterns for RMnO$_3$ (R = Er-Lu) samples prepared by the hydrothermal synthesis method. The indices are for the hexagonal space group *P6$_3$cm*, and the reflection assigned to the K-rich birnessite K$_y$MnO$_w$ impurity (KBi) is indicated. (b) SEM image of two slightly overlapping ErMnO$_3$ crystals in a sample prepared by the hydrothermal synthesis method.

In the orthorhombically-distorted perovskite structure for the larger *R*s, the trivalent Mn cations are located inside corner-sharing MnO$_6$ octahedra as presented in Figure 5.[25,53,I] The stability of the perovskite structure is often evaluated on the basis of the Goldschmidt tolerance parameter (*t*),[54] which provides a numerical measure for the mismatch between ions occupying the two types of cation sites (here *R* and Mn). In an ideal case with no mismatch, t [$=(r_R + r_O)/\sqrt{2}(r_{Mn} + r_O)$] is equal to unity. For the entire series of stoichiometric RMnO$_3$, the Goldschmidt tolerance parameter is lower

than 0.9 which is why the symmetry is lowered from cubic to orthorhombic. The stability limit for the formation of orthorhombic perovskite RMnO$_3$ under ambient conditions is found between R = Dy (t = 0.839) and Ho (t = 0.837).

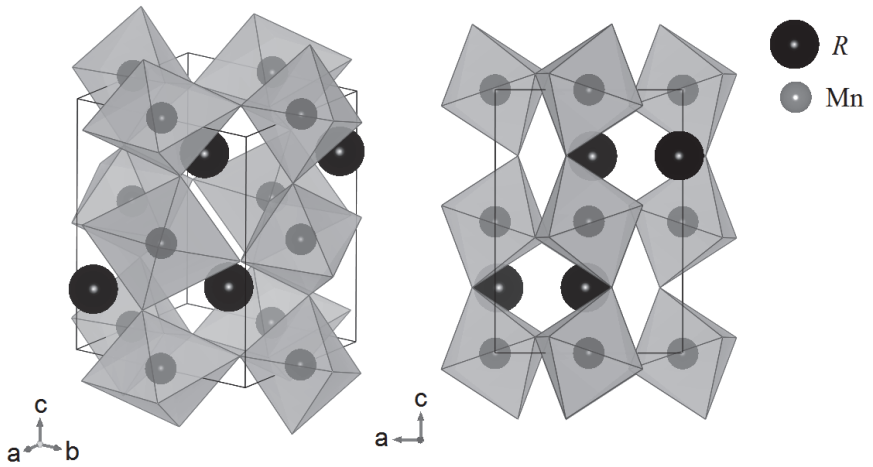

Figure 5. Polyhedral representation of the orthorhombic form of RMnO$_3$. The larger spheres indicate the R^{III} ions and the smaller spheres indicate the Mn^{III} ions. The O^{-II} anions are located at the apexes of the polyhedra.

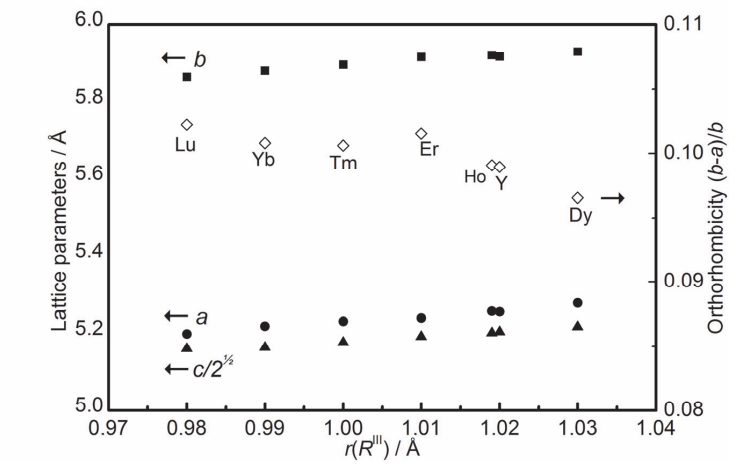

Figure 6. Variation of the lattice parameters and degree of orthorhombicity of o-RMnO$_3$ (R = Y, Dy-Lu) with the ionic radius, $r(R^{III})$.[I] The ionic radii are for the 8-coordinated R^{III} ions.[51,52]

When the ionic radius of R^{III} decreases, the positions of oxygen atoms must be re-adjusted in order to maintain the connections with the *R* atoms. The distortion of the oxygen sublattice leads to increasing tilts of the MnO_6 octahedra, which in turn increases the orthorhombic splitting of the unit-cell dimension as compared to the ideal cubic perovskite structure. In the *o*-$R$$MnO_3$ series, the increase in the degree of orthorhombicity as defined by $(b-a)/b$ with decreasing $r(R^{III})$ is shown in Figure 6.[I] Furthermore, the progressive reduction in the R^{III} size in the *o*-$R$$MnO_3$ perovskite series also results in a decrease in the Mn-O-Mn angle. Figure 7 shows the average Mn-O-Mn angle in *o*-$R$$MnO_3$ as a function of $r(R^{III})$.[I]

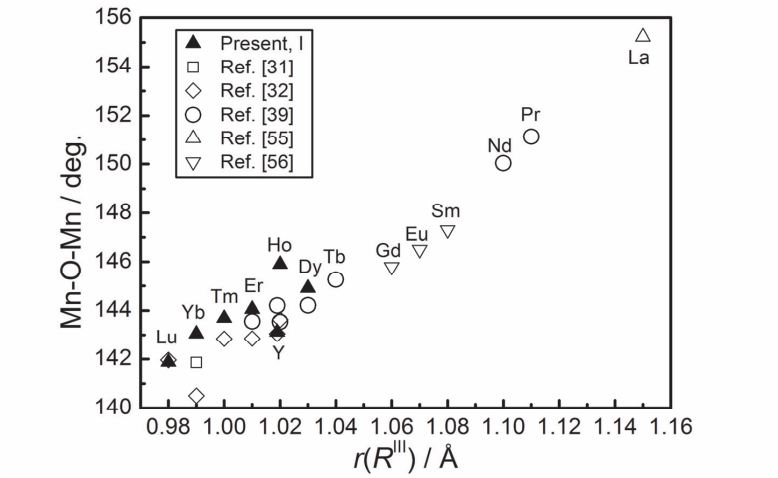

Figure 7. Variation of Mn-O-Mn bond angle of *o*-$R$$MnO_3$ with the ionic radius, $r(R^{III})$.[I]

2.3 Magnetic Properties

The decreasing size of electronic devices has led to increased interest in combining electronic and magnetic properties into multifunctional materials.[57] This way, a single component could perform more than one task. However, designing novel multiferroics that combine magnetic and electrical orderings in the same phase has proven to be quite challenging. The problem has been the contradiction between the usual atomic-level mechanisms driving ferromagnetism and ferroelectricity, as they require

empty and partially filled transition metal orbitals, respectively.[58] Although the ferroelectricity in *h*-*R*MnO_3 is caused by the noncentrosymmetric structure of these compounds, no particular dependency has been observed for the increasing buckling of the *R* plane and the ferroelectric transition temperature (T_{FE}).[59] However, all the members of the *h*-*R*MnO_3 series exhibit a magnetic transition of an antiferromagnetic type, and the Néel temperature (T_N) is increased slightly towards the heavier members of the series. For samples prepared for the present study through the sol-gel method and the high-pressure treatment,[I] the AFM-type transition was found to occur at temperatures between 80 and 90 K as seen in Table 1. At the same time, the increase in the absolute value of the Weiss temperature is rather significant. This phenomenon is not only attributed to the strengthening of the magnetic interactions with the decreasing volume of the unit cell, but also to the geometrical frustration in the two-dimensional triangular Mn-O lattice.[60] To confirm that the HP treatment itself does not affect the studied materials, the properties of as-synthesized and HP-treated *o*-$DyMnO_3$ were compared. As seen in Table 1, there is no significant change in the magnetic properties of *o*-$DyMnO_3$.

Table 1. The Néel and Weiss temperatures together with the effective paramagnetic moments of hexagonal and orthorhombic *R*MnO_3 prepared through the sol-gel method and the high-pressure treatment.[I]

	Unpaired electrons	**Weiss temperature θ [K]**	**Néel temperature T_N [K]**	**Effective paramagnetic moment μ_{eff} [μ_B]**	
Hexagonal (*P6$_3$cm*)				**Observed**	**Theoretical**
Ho	6	-20	~ 80	11.1	11.7
Y	0	-29	~ 80	8.9	4.9
Er	5	-29	~ 80	10.5	10.8
Tm	4	-61	81	8.6	9
Yb	3	-180	87	6.4	6.7
Lu	2	-602	89	5.2	4.9
Orthorhombic (*Pbnm)*					
Dy before HP	7	-20	~ 40	11.5	11.7
Dy after HP	7	-27	~ 40	11.6	11.7
Ho	6	-45	~ 40	12.4	11.7
Y	0	-118	43	5.7	4.9
Er	5	-20	43	10.7	10.8
Tm	4	-59	43	9.8	9.0
Yb	3	-72	43	6.9	6.7
Lu	2	-70	40	4.9	4.9

The members of the *o*-RMnO$_3$ perovskite system are AFM insulators below their Néel temperatures, but the spin configuration changes with the rare-earth species.[61] Although the members of the *o*-RMnO$_3$ series are often mentioned as hosts for the CMR phenomenon, hole-doping is actually needed for the phenomenon to occur.[16,17,45,46,62] The Weiss temperatures of orthorhombic *o*-RMnO$_3$ phases are not likely to follow any specific trend and the values do not differ as strongly from each other as in the case of the *h*-RMnO$_3$ phases. However, as seen in Table 1, the effective paramagnetic moments of both the hexagonal and orthorhombic polymorphs increase with increasing number of unpaired electrons.

The RMnO$_3$ compounds of the larger rare earths (R = La, Pr, Nd) are known to show oxidative nonstoichiometry.[46,63,64] The effect of the oxygen nonstoichiometry on the magnetic properties is rather drastic as the type of magnetic order, magnetic moments and transition temperatures all depend strongly on the oxygen content of these materials. Although the perovskite structure allows the formation of oxygen vacancies, it is not possible to insert excess oxygen into the structure. Thus, the oxygen surplus has to be achieved through the formation of cation vacancies in the structure. As the Mn valence must be adjusted accordingly, the concentration of Mn^{IV} is increased on the expense of Mn^{III}. The presence of Mn^{IV} gives rise to ferromagnetism, improving also the electrical conductivity and colossal magnetoresistance.[15-17] Of the RMnO$_{3+\delta}$ compounds, the nonstoichiometry has been most frequently studied in lanthanum manganite.[46,62,63] Okamoto *et al.*[46] have even extended the work to highly cation-deficient $La_{1-x}Mn_{1-x}O_3$ with $x \approx 0.14$ by means of high-pressure oxygenation techniques. As the degree of cation-deficiency was increased, the ferromagnetic transition temperature (T_C) was found to follow a bell shape with a maximum of 248 K at $x \approx 0.10$. The T_C could be altered quite remarkably, as the lowest Curie temperatures observed were 148 and 151 K for samples with $x \approx 0.12$ and 0.05, respectively.

3 STRUCTURE AND PROPERTIES OF $MnCo_2O_4$ SPINELS

The members of the $(Mn,Co)_3O_4$ spinel system have a variety of applications as materials for catalysts,[21,65-68] sensors,[69] and solid oxide fuel cells (SOFCs).[70-72] Especially the use of $MnCo_2O_4$ as a protective coating on ferritic stainless steel interconnects in SOFCs has gained increasing interest in recent years. Due to the large number of applications, it is not surprising that the possible preparation methods of these spinels have been a subject of intense research. This is the case especially for catalyst purposes to obtain high surface area $MnCo_2O_4$ and for SOFC applications where the production of uniform and pin-hole free thin films is of great importance. Another interesting aspect of $(Mn,Co)_3O_4$ spinels is the magnetic properties which have attracted wide attention due to their unusual hysteresis and magnetization process.[21-24]

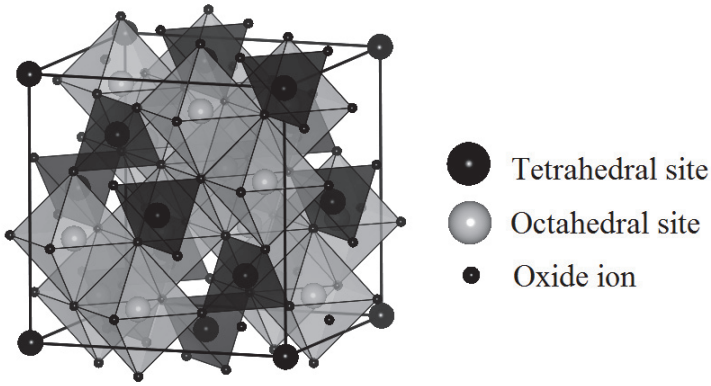

Figure 8. Crystal structure of a spinel, AB_2O_4. The tetrahedral units are presented with darker polyhedra and the octahedral units with lighter polyhedra.

The crystal structure of $MnCo_2O_4$ is that of an inverse spinel, which has a cubic structure belonging to space group $Fd\,\bar{3}\,m$. Spinels form a large class of compounds whose general formula can be written as AB_2O_4, where A and B are metal cations (Figure 8). The unit cell consists of 32 oxide ions in an almost perfectly cubic close-packed arrangement in which the A and B sites are surrounded by tetrahedral and octahedral configurations of oxide ions, respectively. If A is divalent and B is triva-

lent, a normal spinel structure would locate the *A* cations in the tetrahedral sites and all the *B* cations in the octahedral sites. However, in an inverse spinel, the tetrahedrally coordinated sites are occupied by the trivalent cations and the rest of the trivalent along with the divalent cations are located in the octahedral sites.

The debate over the actual distribution of oxidation states of manganese and cobalt in $MnCo_2O_4$ has been going on for decades as research groups have been looking to explain the magnetic properties of these spinels.[22,73-75] In general, the oxygen content of spinels cannot be varied to the same extent as in the case of perovskites, but on the other hand some spinels, such as Co_3O_4, are known for their oxygen nonstoichimetry. Earlier studies on powder samples have shown the possibility to alter the oxygen content of $MnCo_2O_4$. Moreover, the effect of the oxygen content on the magnetic characteristics of $MnCo_2O_{4+\delta}$ has also been studied.[22,23] If prepared at high temperatures $MnCo_2O_4$ has a structure of a cation-deficient spinel, but low-temperature synthesis conditions ensure an increased oxygen-to-metal ratio. The Curie temperature of ferrimagnetic $MnCo_2O_{4+\delta}$ (or $Mn_{1-x}Co_{2-2x}O_4$) has been found to decrease remarkably with increasing oxygen content (or increasing cation-vacancy concentration).[22] According to Bazuev *et al*.[22], the Curie temperature decreased from 183 K of the stoichiometric spinel to 167.5 K for $MnCo_2O_{4.275}$ and 67.5 K for $MnCo_2O_{4.62}$.

4 ALD OF TERNARY MANGANESE OXIDE MATERIALS

Atomic layer deposition offers an excellent method for producing a coating that is not only uniform and conformal on large uneven surfaces, but it is a technique that enables excellent control of the thickness and stoichiometry of the film.[11,12] The benefits of ALD are mainly derived from the self-limiting growth mechanism, which is achieved through alternate pulsing of the precursors. Majority of ALD processes involves binary reaction sequences in which two types of surface reactions result in the deposition of a binary compound. After each reactant pulse, the excess reactant and reaction products are removed from the reactor chamber. Thus, gas-phase reactions are eliminated and the growth proceeds exclusively *via* surface reactions. The basic idea of ALD is quite fascinating in its simplicity. On a closer look, however, a world of challenges is revealed as the slowness of the method is tackled through design of efficient reactors and proper precursor chemistry.

The number of ternary and more complex oxide processes developed for ALD has been steadily increasing in recent years. Several studies have already shown the feasibility of depositing ternary oxides and other multicomponent phases with excellent control of cation stoichiometry.[76-81,**II**,**IV**] The current trend towards more and more ambitious ALD processing emphasizes the role of ALD as a link between laboratory conditions and real-life applications. Especially, as the selection of these materials includes rather exciting materials solutions such as materials for solid oxide fuel cells[79,82,**III**] and all-solid-state lithium ion batteries[83]. In the present work, a method has been developed for fabricating spinel-structured $MnCo_2O_{4+\delta}$, and both hexagonal and orthorhombic $R$$MnO_3$ thin films through ALD and post-deposition heat treatment.[**II-IV**]

4.1 ALD of the *R*MnO_3 Series

The fabrication of $R_xMn_yO_3$ thin films by ALD using $R(thd)_3$ (thd = 2,2,6,6-tetramethyl-heptane-3,5-dionate), $Mn(thd)_3$ and ozone as precursors was successful for the entire series. The films were of high-quality showing no significant gradients

in either thickness or Mn content.[II,IV] The deposition temperature was varied between 225 and 350 °C as seen in Table 2. However, most of the depositions were performed at 275 °C. The metal precursors were chosen based on the possibility to in-house synthesis and easy handling due to excellent stability in air.

Table 2. Deposition temperatures (T_{dep}) and precursor ($R(thd)_3$) evaporation temperatures (T_{sub}) used in the depositions of $R_xMn_yO_3$ thin films. The growth-per-cycle (GPC) values are for the $RMnO_3$ films deposited at 275 °C with a *R*:Mn pulsing ratio of 1:1.[IV]

R	T_{sub} / °C	T_{dep} / °C	GPC / Åcycle^{-1}
La	162	275	0.23
Sm	139-141	275	0.23
Tb	128-130	250-325	0.18
Y	123	225-350	0.18
Er	127	275	0.18
Tm	126	275	0.18
Yb	123	275-300	0.18
Lu	123	275-300	0.18

The growth-per-cycle (GPC) values were calculated by dividing the film thickness by the number of basic ALD cycles used. In the case of $RMnO_3$ thin films, a basic ALD cycle consisted of the following sequence: 1.5 s $R(thd)_3$ followed by 1.5 s purge or 2.0 s $Mn(thd)_3$ followed by 2.0 s purge, 1.5 s ozone and 1.8 s purge. The GPC values were found to decrease with decreasing size of the rare-earth constituent. The effect is similar, although slightly less significant as observed for rare-earth scandates.[84] It is well known that the GPCs of binary rare-earth oxides increase with increasing size of ionic radius $r(R^{III})$ from 0.21 Å/cycle for Tm up to 0.44 Å/cycle for Nd.[85,86] The GPC is increased not only because of the increasing size of the *R* constituent but also due to other factors including the tendency of larger rare earths to adopt higher coordination numbers leading to dimerization of their $R(thd)_3$ complexes.[87-89] In the case of the $RMnO_3$ series, the increase in GPC is somewhat less pronounced compared to binary rare-earth oxides, but still greater than what can be explained simply by the increasing ionic radius.

The linear dependence of $Y_xMn_yO_3$ film thickness on the number of basic ALD cycles (deposited at 275 °C) is demonstrated in the right panel of Figure 9. The con-

stant GPC value confirms that the thickness of the films can be controlled simply by the number of deposition cycles. Depositions performed at 275 °C showed moreover excellent control of the cation stoichiometry as seen in Figure 9 for R = Yb, Y and Tb. Although it is often found that the film composition has a slightly non-linear dependency on the ALD precursor pulsing ratio, in the case of $R_xMn_yO_3$ (with R = Tb, Yb), this dependency is extremely close to linear. Even highly Mn-rich films (with Mn content up to 88 %) could be deposited in a well-controlled manner if the temperature was kept at 275 °C or below and the ozone pulsing was sufficient.

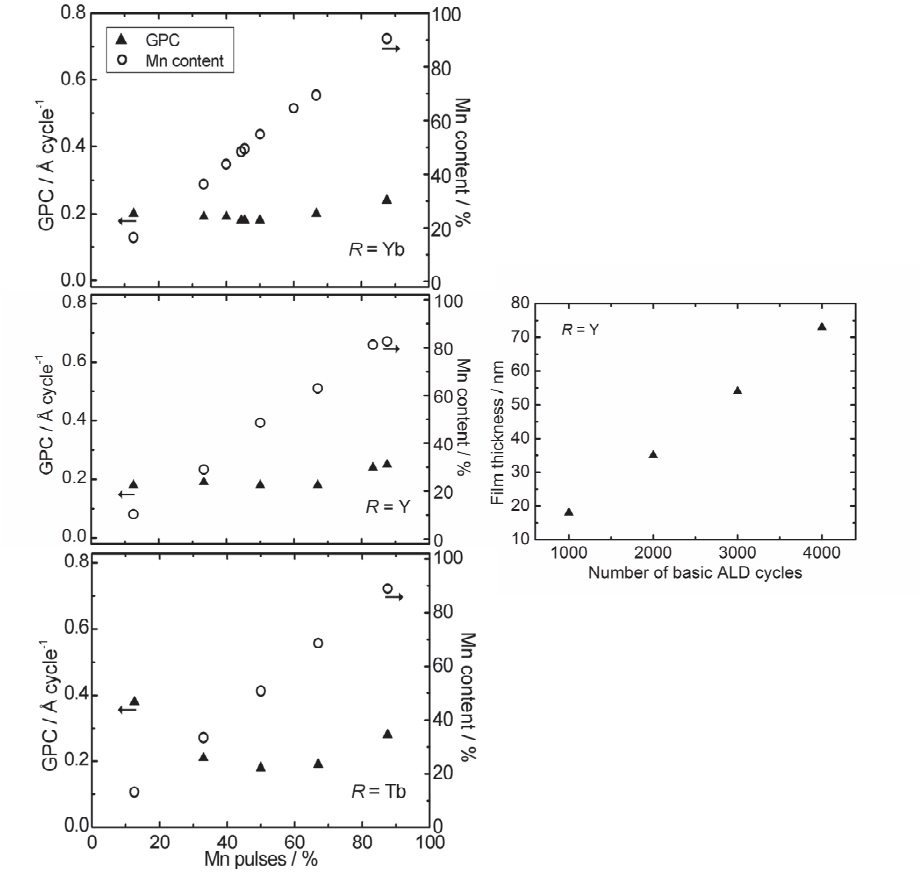

Figure 9. Effect of the precursor pulsing ratio on the actual Mn content (○) and the growth-per-cycle value (▲) of $R_xMn_yO_3$ (R = Yb, Y, Tb) films at the deposition temperature of 275 °C (left panel). The dependence of the $YMnO_3$ (with a Y:Mn pulsing ratio of 1:1) film thickness on the number of basic ALD cycles (right panel).[IV]

Although the studies on ternary and more complex oxide processes are generally based on some previous work on binary oxides, an ALD process of a ternary oxide material is often much more than just the sum of two binary processes. At the same time, any experience on the constituent binary oxides should not be ignored as it may well contain explanations for detected anomalies in the ternary oxide process at hand. An interesting example is that of terbium oxide, as any well-controlled ALD growth of the binary terbium oxide remains to be achieved but it is possible to deposit the ternary manganite, $Tb_xMn_yO_3$, with excellent control of the film composition.[IV] As seen in the bottom panel of Figure 9, the dependency of film composition on the ALD pulsing ratio is extremely close to linear. Therefore, a specific film composition can clearly be easily achieved. At the same time, there is a considerable increase in the GPC value while depositing highly terbium-rich $Tb_xMn_yO_3$ films. X-ray diffraction (XRD) analysis performed on as-deposited samples revealed the presence of terbium oxide in the films. In fact, terbium oxide was the only crystalline phase detected in any of the as-deposited $R_xMn_yO_3$ films. Thus, it is clear that the $Tb_xMn_yO_3$ differs from the rest of the $R_xMn_yO_3$ series studied in this work and the reason seems to be found in the uncontrolled growth of the binary terbium oxide. In fact, a few depositions of TbO_x were performed even in this study and, as the films were visibly thinner towards the edges of the substrate, it became evident that no well-controlled growth could be observed at the attempted temperature range of 250-325 °C. The GPC of terbium oxide at 275 °C was found to be ~0.6 Å/cycle, which would well explain the observation of increasing GPC of $Tb_xMn_yO_3$ with increasing Tb content. However, rather than stating that the ALD-type growth of $Tb_xMn_yO_3$ cannot be achieved, one should consider the excellent control of the film composition and the high-quality result with no significant thickness gradients. Moreover, if the film composition is kept close to stoichiometric, the GPC is under control, as well.

4.2 Control of the Film Composition in $(Mn,Co)_3O_4$

The film composition of ternary oxide films often has a consistent but slightly non-linear dependency on the ALD precursor pulsing ratio. A linear dependency can be observed only if the metal precursors are similar in size and surface reactivity as is

the case with the RMnO$_3$ thin films deposited using R(thd)$_3$, Mn(thd)$_3$ and ozone.[II,IV] The effect of the Mn:Co pulsing ratio on the composition and the GPC of (Mn,Co)$_3$O$_4$ films deposited at 150 °C is illustrated in Figure 10.

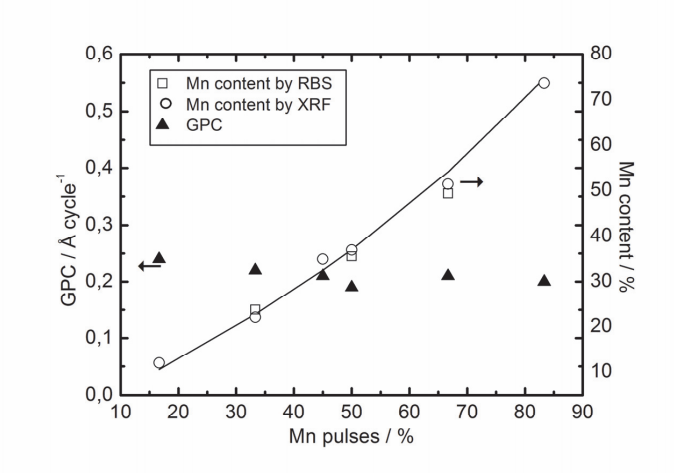

Figure 10. Effect of the pulsing fraction of Mn(thd)$_3$ on the Mn content (by XRF and RBS) and the GPC of (Mn,Co)$_3$O$_4$ films at the deposition temperature of 150 °C (the thickness of the films was 35-50 nm).[III]

According to both X-ray fluoresence (XRF) and Rutherford backscattering spectrometry (RBS) analyses, the dependency of the measured Mn:Co ratio on the pulsing ratio is not quite linear.[III] Nonetheless, the cation stoichiometry was easily controlled by a simple adjustment of the pulsing ratio. Furthermore, the film quality and the cation stoichiometry were maintained while depositing even much thicker films, *i.e.* 280 nm, indicating an exclusively surface-reaction-controlled ALD process. As seen in Figure 10, the deposition of cobalt is slightly amplified in comparison to manganese. According to Lie *et al.*[90], a very natural explanation could be the adsorption of Co(thd)$_2$ precursor molecules as Co(thd) while Mn(thd)$_3$ is more likely adsorbed as Mn(thd)$_2$.

The composition of (Mn,Co)$_3$O$_4$ films was well under control in the temperature range of 140-160 °C, which could be identified as the 'ALD window' or the temperature range of essentially constant GPC value for this process. The ALD window ob-

served for $(Mn,Co)_3O_4$ was very narrow considering the corresponding temperature windows of the binary processes, Co_3O_4 and MnO_x, with ALD-type growth in the temperature ranges, 114-307 °C [91,92] and 138-210 °C[93], respectively. The lower limit of 140 °C for $(Mn,Co)_3O_4$ is certainly explained by the lower limit of the growth of MnO_x; then, however, above 160 °C the film quality deteriorated drastically resulting in films with serious thickness variations and poor adhesion. Moreover it was revealed that at higher temperatures the GPC value of the films increased rapidly with increasing temperature. In Figure 11, the GPC value and the Mn content are plotted for approximately 40 nm thick $(Mn,Co)_3O_4$ films grown with a cation pulsing ratio of Mn:Co = 1:1. At 175 °C the GPC value is already 2.5 times higher than within the ALD window and above 200 °C even seven times greater GPC values were observed (not shown in Figure 11) indicating a complete lack of control of the film growth. Generally, such a significant increase in the GPC value would be an indication of the decomposition of the precursors. However, no similar problems were encountered in the deposition of binary manganese and cobalt oxides.[91-93]

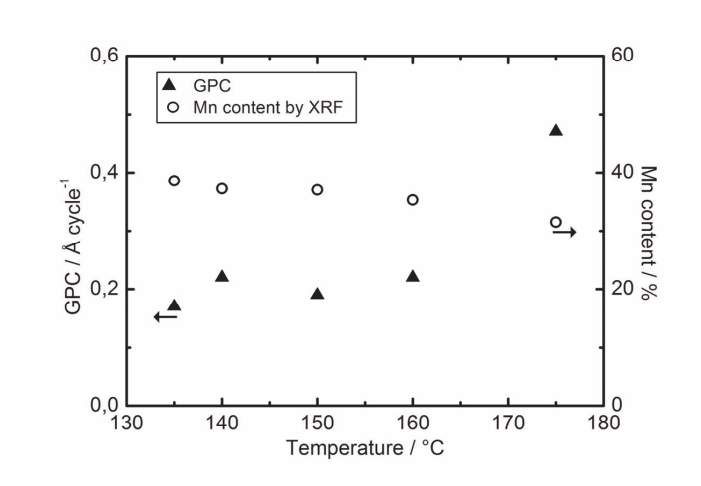

Figure 11. Temperature dependences of the GPC value and the Mn content (against the total metal content) for $(Mn,Co)_3O_4$ films deposited with a Mn:Co pulsing ratio of 1:1 (the number of basic ALD cycles was 2000).[III]

4.3 Challenges of the Ternary Manganese Oxide Processes

The excellent control of the film composition, especially in the case of the RMnO$_3$ series, gives a reason to believe that the deposition of ternary manganese oxides could be performed despite the several challenges encountered. One of the main challenges with any ALD process is to separate the weaknesses of the process from those of the reactor. One of the main problems of the ALD processes of ternary manganese oxides presented in this study is the fact that manganese oxide is a well-known catalyst for the decomposition of ozone.[93,94] What makes the situation even more interesting considering the (Mn,Co)$_3$O$_4$ films, is the fact that cobalt oxide has the same function as well.[94] Preliminary depositions of RMnO$_3$ samples[I] did not show promising results, especially if the samples contained increased amounts of manganese. One of the most obvious explanations at hand was the problem with the decomposition of ozone, but later results[IV] (seen in Figure 9) proved this explanation to be insufficient. The film composition could, in fact, be controlled extremely well. The only problem was the increase in the GPC value observed for films with higher Mn contents (deposited at 275 °C). Interestingly, similar effect was not observed for (Mn,Co)$_3$O$_4$ films deposited at a much lower temperature of 150 °C (Figure 10). As the decomposition of ozone is increased with increasing temperature, it is quite possible that the ternary manganese oxide materials studied here do catalyze the decomposition of ozone. However, the effect seems to be minor and the ALD growth of *e.g.* stoichiometric RMnO$_3$ samples is possible.

The slight but steady increase in Mn content with increasing deposition temperature was another problematic observation of the ALD processes of the RMnO$_3$ series. As seen in Figure 12, the ALD processes of these ternary manganites seem to be sensitive to changes in temperature. Fortunately, the changes in Mn content and GPC are not too significant, and moreover, it should be noted that the processes are reproducible at a specific temperature as long as the heating of the ALD reactor is reliable and reproducible. Any changes in reactor configuration tend to affect the cation ratio of the films; however, the dependency between the film composition and the ALD pulsing ratio should not be affected. In the case of RMnO$_3$, the film composition should

always have a close to linear dependency on the ALD pulsing ratio, thus, depositing a film with a specific composition should be rather a straight-forward task to achieve.

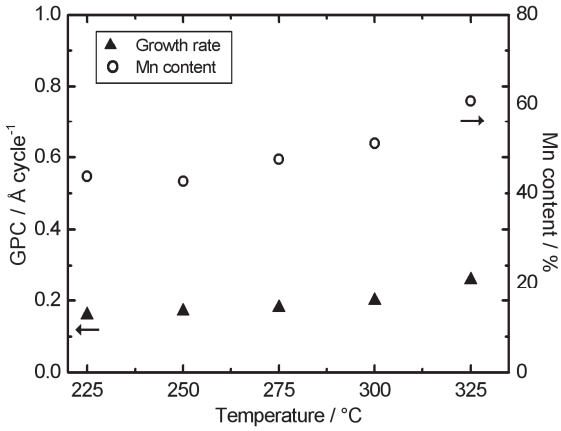

Figure 12. Temperature dependencies of the growth-per-cycle (GPC) value (triangles) and the Mn content (circles) for $Y_xMn_yO_3$ deposited with a Y:Mn pulsing ratio of 1:1 (the number of basic ALD cycles was 2000).

5 HEXAGONAL AND ORTHORHOMBIC *R*MnO_3 THIN FILMS

Epitaxial phase stabilization is a practical tool of solid-state chemistry that can be used to construct new structures despite of their instability in bulk form. It is a technique in which a thin film can be forced to adopt a specific crystal structure or an orientation through appropriate choice of substrate crystal. Epitaxial stabilization is based on free-energy gain due to structural coherence at the film/substrate interface. As a result, severe synthesis conditions, such as ultra-high pressures, can be avoided and the preparation of metastable phases is possible in much milder conditions. In some cases, epitaxial stabilization may even be the only way to stabilize thermodynamically unstable structures, as is the case for metastable *h*-*R*MnO_3 with larger rare-earths.[47-49] Epitaxial stabilization can be used to control the orientation of the film,[92,II] to stabilize metastable phases,[95-97] to stabilize metastable polymorphs without changing the stoichiometry of the compound[98,II,IV] or to stabilize metastable polymorphs with a simultaneous change in the metal oxidation state.[99-102] In the present study, a technique was developed for the fabrication of hexagonal and metastable orthorhombic *R*MnO_3 thin films through ALD and subsequent heat-treatment. The formation of the metastable *o*-*R*MnO_3 was enhanced through depositions of high-quality thin films on coherent perovskite substrates; $LaAlO_3$(100) and $SrTiO_3$(100).

5.1 Structural Properties of *R*MnO_3 Thin Films

Low deposition temperatures of ALD often result in an amorphous structure of the as-deposited ternary oxide films.[84,103-105] The cation-stoichiometric thin films of the *R*MnO_3 series deposited at 225-325 °C were all amorphous after the deposition.[II,IV] Therefore, a post-deposition heat treatment was performed for the samples deposited at 275 °C. In fact, the only crystalline phase detected in the as-deposited samples was the binary terbium oxide found in the terbium-rich $Tb_xMn_yO_3$ films. The size of the rare-earth element was found not to have a major effect on the temperature at which the *R*MnO_3 films were crystallized. The crystallization temperatures varied between 650-900 °C. However, as an example, $YbMnO_3$ and $TbMnO_3$ deposited on $SrTiO_3$ both crystallized at 850 °C. The substrate material appeared to have some effect on

the crystallization temperature with silicon substrate generally requiring a slightly higher annealing temperature. The resulting crystal structures of RMnO$_3$ are shown in Table 3 for films deposited on silicon, LaAlO$_3$ and SrTiO$_3$.

Table 3. Effect of the substrate material on the crystal structure of RMnO$_3$ with R = Y, La, Sm, Tb, Er-Lu (after post-deposition annealing in N$_2$).[IV]

R	**Deposited on Si**	**Deposited on LaAlO$_3$**	**Deposited on SrTiO$_3$**
La	*r*-LaMnO$_3$	*r*-LaMnO$_3$	-
Sm	*o*-SmMnO$_3$	*o*-SmMnO$_3$	*o*-SmMnO$_3$
Tb	*o*-TbMnO$_3$	*o*-TbMnO$_3$	$Tb_2Mn_2O_7$ or $TbMn_2O_5$
Y	*h*-YMnO$_3$, Y_2O_3, MnO_2, Mn_2O_3	*o*-YMnO$_3$	*o*-YMnO$_3$
Er	*h*-ErMnO$_3$	-	-
Tm	*h*-TmMnO$_3$	-	-
Yb	*h*-YbMnO$_3$	*o*-YbMnO$_3$	*o*-YbMnO$_3$, *h*-YbMnO$_3$
Lu	*h*-LuMnO$_3$	*o*-LuMnO$_3$	-

According to calculations on film/substrate mismatch of RMnO$_3$ and the perovskite substrates LaAlO$_3$ and SrTiO$_3$, the low mismatch with lanthanum aluminate should be the best promoter for the formation of metastable *o*-RMnO$_3$ perovskites.[36] The average lattice mismatch with average lattice parameter $\bar{a} = \sqrt[3]{abc/4}$, and mismatch given as $M = \left|(\bar{a}/a_s) - 1\right|$ calculated for both the perovskite substrates is shown in Figure 13, which has been adapted from Ref. 36. The mismatch between the RMnO$_3$ film and the substrate causes compression-type strain to the film in the case of LaAlO$_3$ and tension-type strain in the case of SrTiO$_3$. The most successful results on stabilization of the *o*-RMnO$_3$ perovskites with the small R constituents were indeed obtained when depositing the film on LaAlO$_3$ (Table 3). In fact, single-phase RMnO$_3$ perovskite samples were obtained on LaAlO$_3$ for all the investigated rare-earth constituents. A successful example of YbMnO$_3$ is presented in Figure 14, in which the XRD patterns for YbMnO$_3$ films deposited on silicon, LaAlO$_3$ and SrTiO$_3$ are shown.

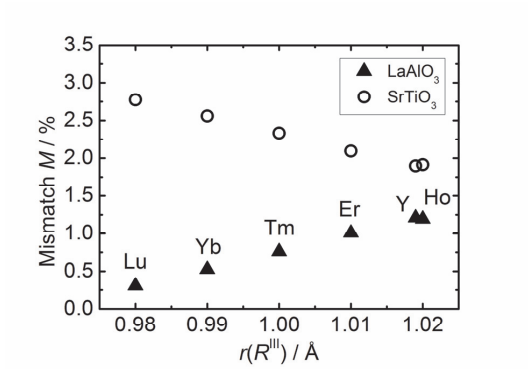

Figure 13. Average lattice mismatch calculated for $SrTiO_3$ and $LaAlO_3$ substrates.[36]

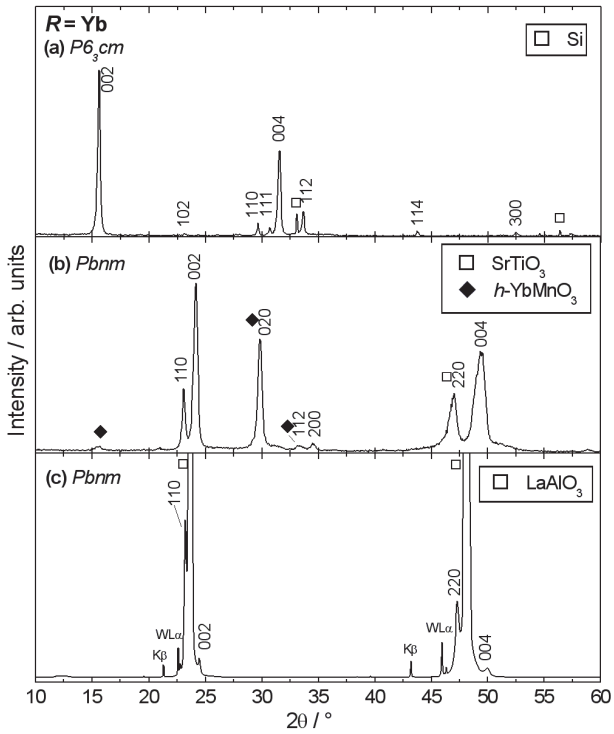

Figure 14. XRD patterns for annealed $YbMnO_3$ films deposited on (a) Si(100), (b) $SrTiO_3$(100), and (c) $LaAlO_3$(100) substrates. The indices are for the hexagonal space group $P6_3cm$ in (a) and for the orthorhombic space group *Pbnm* in (b) and (c). The film thickness was 200 nm.[IV]

As seen in Figure 14, orthorhombic $YbMnO_3$ contained minor amounts of hexagonal impurity when deposited on $SrTiO_3$, whereas the film deposited on $LaAlO_3$ was of single-phase *o*-$YbMnO_3$. Hexagonal $YbMnO_3$ was obtained on silicon at 900 °C, but was found to decompose at 1000 °C forming binary oxide impurities. Similar behavior was observed for *h*-$LuMnO_3$ as well, even though higher temperatures are known to favor the formation of the hexagonal structure in bulk samples.[38,39,I]

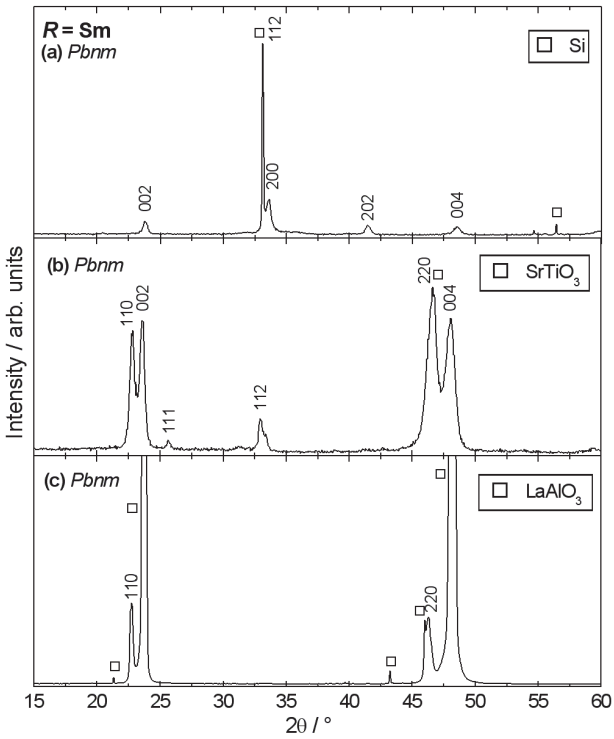

Figure 15. XRD patterns for annealed $SmMnO_3$ films deposited on (a) Si(100), (b) $SrTiO_3$(100), and (c) $LaAlO_3$(100) substrates. The indices are for the orthorhombic space group *Pbnm*. The film thickness was 200 nm.[IV]

Not surprisingly, the crystal structures for the larger rare earths were less affected by the selection of substrate crystals used and, as presented in Figure 15, single-phase orthorhombic $SmMnO_3$ was obtained on all the attempted substrates. An exception to the rule was given by $TbMnO_3$ deposited on $SrTiO_3$ which resulted in the formation

of either $Tb_2Mn_2O_7$ or $TbMn_2O_5$. Moreover, the distinction between orthorhombic and rhombohedral perovskite structures of $LaMnO_3$ was rather challenging considering the methods available, but the preparation conditions, including the presence of ozone, are likely to favor the formation of rhombohedral, cation-deficient $LaMnO_{3+\delta}$. In general, the crystal structure of RMnO$_3$ could be well controlled by simply choosing an appropriate substrate crystal, and the minor amounts of impurities observed in the samples consisted of either binary oxide impurities or hexagonal phase of the RMnO$_3$ in question.

5.2 Magnetic Properties of *R*MnO$_3$ Thin Films

The temperature dependencies of magnetization measured with a superconducting quantum interference device (SQUID) in both zero-field-cooled (ZFC) and field-cooled (FC) modes for the $SmMnO_3$ thin-film samples deposited on silicon, $LaAlO_3$ and $SrTiO_3$ are shown in Figure 16.[IV] The observed Néel temperature is ~60 K in all the cases regardless of the substrate material and well in agreement with results on powder samples.[106]

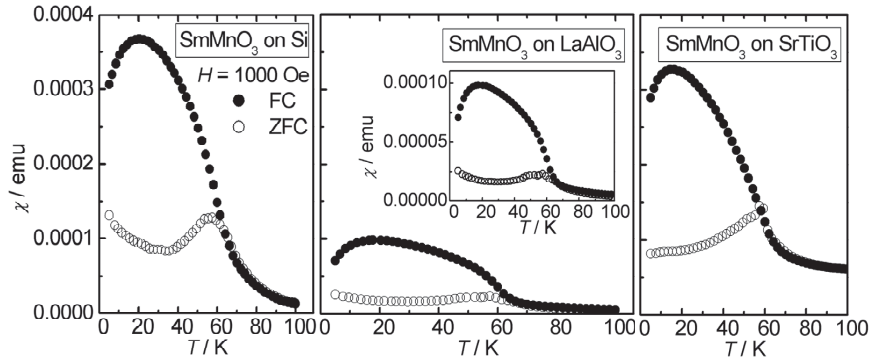

Figure 16. Temperature dependence of magnetic susceptibility (χ) in ZFC and FC modes under an external field of 1000 Oe for $SmMnO_3$ thin-film samples deposited on silicon, $LaAlO_3$ and $SrTiO_3$.[IV]

Most of the measurements in the present work were performed on RMnO$_3$ samples deposited on $LaAlO_3$ as these samples contained the least amount of impurities. The

poor crystallinity of hexagonal phases and some technical difficulties with the extremely sensitive equipment caused some difficulties in the magnetization measurements and collecting good-quality data proved to be challenging despite several attempts. Moreover, although qualitative interpretations based on magnetization measurements of thin-film samples can be done reliably, care should be taken while making any conclusions based on absolute values obtained from the data as several factors, such as the degree of crystallinity of the film, can affect the magnitude of the magnetic susceptibility. For *o*-RMnO$_3$ the temperature dependence of magnetization revealed the expected antiferromagnetic properties as seen in Figure 17 where *o*-YMnO$_3$ and *o*-TbMnO$_3$ were chosen as representative examples. The Néel temperature for both *o*-YMnO$_3$ deposited on LaAlO$_3$ and *o*-TbMnO$_3$ deposited on silicon is 40 K which is in good accordance with studies performed on powder samples.[50,107] The magnetization measurements (Figure 17) showed ferromagnetic interactions in the LaMnO$_{3+\delta}$ sample below the Curie temperature of 175 K giving reason to believe that the sample preparation through ALD and subsequent annealing at 1000 °C in N_2 flow does not result in a stoichiometric sample.

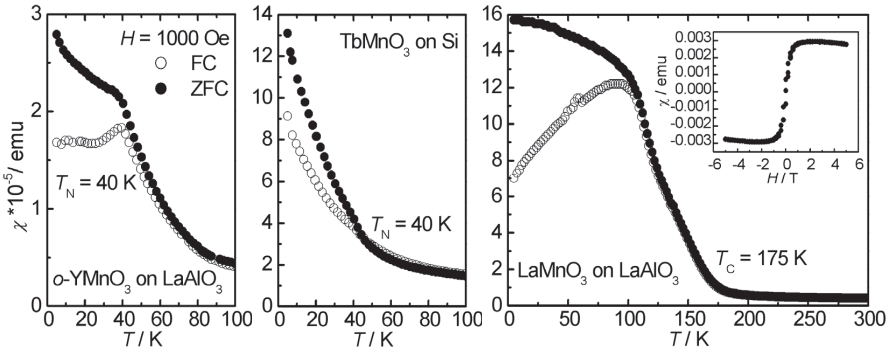

Figure 17. Temperature dependence of magnetic susceptibility (χ) in ZFC and FC modes under an external field of 1000 Oe for *o*-YMnO$_3$ on LaAlO$_3$, TbMnO$_3$ on silicon and LaMnO$_{3+\delta}$ on LaAlO$_3$. The inset: field dependence of magnetic susceptibility (measured at 5 K) of a LaMnO$_{3+\delta}$ film deposited on LaAlO$_3$.[IV]

In order to confirm that the oxygen nonstoichiometry of LaMnO$_3$ thin films can be easily affected through alterations in the annealing conditions, the lattice parameters of LaMnO$_3$ samples (deposited on silicon) annealed at 800 °C in nitrogen and oxygen

flow were determined. A slight deviation was indeed observed in the lattice parameters of rhombohedral-type structure[108,109] with a and α increasing from 5.434(8) Å and 60.519(6) ° (O_2 flow) to 5.450(1) Å and 60.610(2) ° (N_2 flow) with decreasing partial pressure of oxygen thus indicating a decrease in oxygen content/the concentration of cation vacancies in the structure.

6 OXYGEN-CONTENT CONTROL IN $MnCo_2O_{4+\delta}$ THIN FILMS

Compared to the control of the cation ratio, the control of oxygen stoichiometry in ALD-grown and other thin-film samples is clearly a less studied problem. Access to methods for studying the oxygen content of a truly thin film is much more limited compared to bulk materials, where *e.g.* redox titration is an extremely feasible solution. The case of the cation-deficient $Mn_{1-x}Co_{2-2x}O_4$ or $MnCo_2O_{4+\delta}$ system offers an interesting example of controlling the oxygen stoichiometry of a thin film sample. The information on the oxygen nonstoichiometry of $MnCo_2O_{4+\delta}$ is vital when it comes to understanding the magnetic properties of these spinels as the magnetic characteristics of $MnCo_2O_{4+\delta}$ are strongly dependent on the oxidation states of manganese and cobalt. Previous work on powder samples by Bazuev *et al.*[22] has shown a remarkable increase in the Curie temperature of ferrimagnetic $MnCo_2O_{4+\delta}$ with decreasing oxygen content (or cation-vacancy concentration). Thus, it is clear that while studying the magnetic properties of such compounds the possibility for alterations in oxygen stoichiometry should always be acknowledged. If $MnCo_2O_{4+\delta}$ is prepared through ALD using $Mn(thd)_3$, $Co(thd)_2$ and ozone as precursors, the precursor chemistry implies oxidation states +III for manganese and +II for cobalt. However, considering the fact that the $MnCo_2O_{4+\delta}$ spinel structure allows changes in its oxygen content and moreover the presence of such a strong oxidizer as ozone, very few assumptions can be made on the oxygen content of the as-deposited films. This is the case especially when ALD is employed as a deposition method due to the exceptionally low deposition temperature. Low-temperature synthesis of $MnCo_2O_{4+\delta}$ results in an increased oxygen-to-metal ratio, whereas the cation-vacancy concentration is decreased towards higher temperatures. Although controlling the oxygen content of bulk samples has been studied for decades, the oxygen control of thin films deposited by ALD has not been reported earlier.

Thin films of $MnCo_2O_{4+\delta}$ grown by ALD at 275 °C crystallized in the cubic spinel structure with space group $Fd\,\bar{3}\,m$.[III] Weak reflections of the spinel structure were observed for the as-deposited films without a trace of binary oxide impurities, as seen in Figure 18. Post-deposition annealing improved the crystal quality of the films

and it was clearly verified that all the diffraction peaks could be indexed in the cubic cell for spinel compounds.

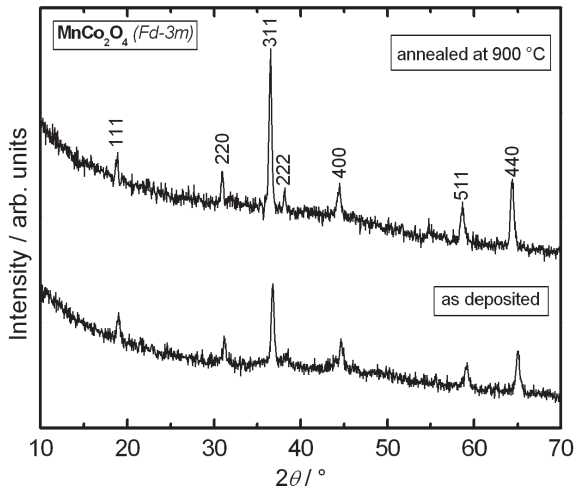

Figure 18. XRD patterns for as-deposited and post-deposition annealed (in air at 900 °C) $MnCo_2O_{4+\delta}$ films. The indices are for the cubic space group $Fd\bar{3}m$.[III]

For the annealed films a gradual increase in the lattice parameter *a* was detected with increasing annealing temperature (Figure 19) from 8.11 Å for the as-deposited films to 8.26 Å for films annealed at 800 °C in N_2 gas flow. The observed magnitude of lattice contraction well agrees with data reported for bulk $MnCo_2O_{4+\delta}$ samples.[110] The increase in lattice parameter *a* and accordingly in unit-cell volume reflects the decrease in oxygen content (or in the oxygen to metal content ratio).[22,110] Loss of the excessive oxygen from the spinel structure of $MnCo_2O_4$ results in the progressive reduction of manganese (Mn^{IV} to Mn^{III}) and/or cobalt (Co^{III} to Co^{II}).[22, 73-75] From Figure 19, compared to annealing in N_2 the increase in the unit cell volume and hence the degree of reduction is somewhat less pronounced when the heat treatment is performed in air. Here it should also be mentioned that annealing in N_2 at 900 °C decomposed the spinel structure, while air-annealing at the same temperature did not result in any noticeable changes in sample quality.

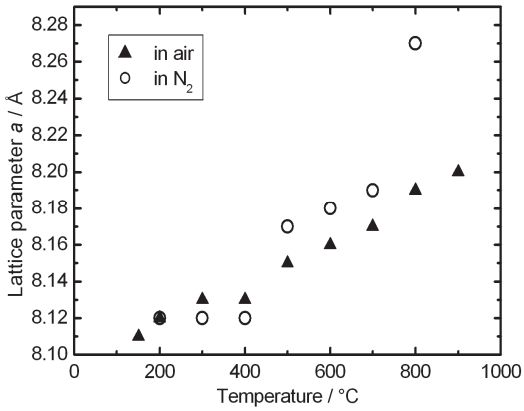

Figure 19. Increase in the lattice parameter *a* with increasing post-deposition annealing temperature for the $MnCo_2O_{4+\delta}$ films. The triangles indicate the values for the films annealed in air and the circles show the values for the films annealed in N_2 gas flow.[III]

In order to further study the effect of the post-deposition annealing conditions, and thus, the changing oxygen content on the magnetic properties of $MnCo_2O_{4+\delta}$ films, the temperature dependence of magnetic susceptibility (χ) was measured for various $MnCo_2O_{4+\delta}$ thin-film samples with measured Mn:Co ratio = 1:2. Figure 20 displays the data for two representative samples, a film annealed at 500 °C in air and a film annealed at 700 °C in N_2 gas flow. As expected, the T_C value of the ferrimagnetic $MnCo_2O_{4+\delta}$ was affected by the conditions of the post-deposition heat treatment. The magnetic measurements revealed an increasing trend in T_C with decreasing *a* parameter (see the inset of Figure 20), confirming that the oxygen stoichiometry indeed had been successfully controlled in the spinel-structured $MnCo_2O_{4+\delta}$ thin films through the post-deposition heat treatments.

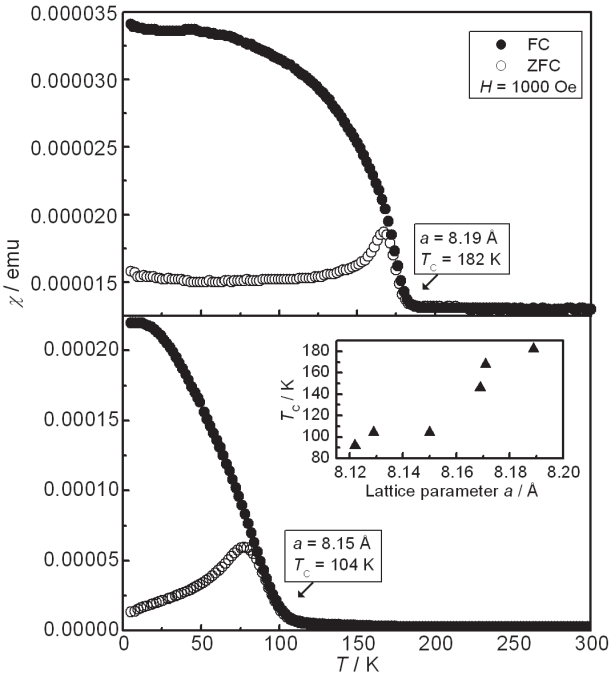

Figure 20. Temperature (T) dependence of magnetic susceptibility (χ) for $MnCo_2O_{4+\delta}$ thin films annealed at 500 °C in air (lower panel) and at 700 °C in N_2 gas flow (upper panel). The inset shows the variation of the Curie temperature of $MnCo_2O_{4+\delta}$ with the lattice parameter a.[III]

7 SOFC APPLICATION OF ALD-GROWN $MnCo_2O_4$

The members of the $(Mn,Co)_3O_4$ spinel system are among the most promising candidates to be used as protective layers on the ferritic stainless steel interconnects of solid oxide fuel cells.[70-72] After several studies on potential protection layers with perovskite structures, *e.g.* (La, Sr)MO_3 (M = Cr, Mn, Fe, Co),[111-115] the focus has lately shifted towards spinel compositions.

Despite the substantial improvement in surface stability of bulk interconnect materials, it has become evident that the use of high-temperature oxidation-resistant alloys has its limitations in terms of satisfactory lifetime and surface stability at the temperatures allowed by current SOFC technologies. Especially chromia-forming ferritic stainless steels have appeared an attractive solution for SOFC interconnect materials due to their electrically conducting oxide scale formation (Cr_2O_3), suitable thermal expansion coefficient, excellent workability and low cost.[116] However, the migration and evaporation of Cr through the chromia scale into SOFC cathodes is a serious issue that degrades the cell performance and limits the long-term application of these alloys. Ferritic stainless steels specifically developed for SOFC applications (Cr-content ~22 %), such as ZMG232L (Hitachi Metals®) and Crofer22 APU (ThyssenKrupp®), have offered some improvement, but the Cr volatility remains unacceptably high.[117,118]

Considering the constant struggle with the surface stability of bulk interconnect materials, it is not surprising that the surface modification of metallic interconnects through application of ceramic protective coating has gained increasing interest. In the development of such coating materials it is highly important to meet the requirements of both high electrical conductivity and low chromium/oxygen diffusivity.[71,119] The protection layer serves as a barrier in preventing Cr migration while simultaneously minimizing the interfacial contact area specific resistance (ASR) between the cathode and the interconnect by limiting the growth of Cr-rich oxide scale with a relatively low conductivity. One of the main challenges in the use of perovskite-structured protective layers is high growth rate of the oxide scale caused by the high oxygen ion conductivity of the perovskites.[119] The scale formation is fairly effec-

tivily inhibited by the use of chromites, which exhibit a lower oxygen ion conductivity than many perovskites. However, Cr vaporization is a concern that complicates the use of all the thus far developed perovskite protective layers.[70,115,120] The promising feature of $(Mn,Co)_3O_4$ spinels as a barrier to Cr migration was first indicated by the work of Larring and Norby[70]. Later studies have supported the observation by showing the effectiveness of $(Mn,Co)_3O_4$ spinels in improving the surface stability of ferritic stainless steel interconnects, minimizing contact resistance and sealing off chromium in the metal substrates.[70-72,121,122]

In the present study the deposition of $MnCo_2O_4$ thin films was tested on stainless steel in addition to silicon substrates. According to the preliminary experiments performed on Crofer22 APU substrates, the growth of $MnCo_2O_4$ showed promising results. A simple tape test was used to test the film adherence to the steel substrate, and although further studies are required, the $MnCo_2O_4$ film remained well intact. In this study the steel substrates were cleaned in ultra-sonic bath using ethanol as a solvent, however, comparisons of other pretreatment methods might offer an excellent possibility to further improve the ALD processing of $MnCo_2O_4$ coatings for SOFC interconnects.

The as-deposited samples of $MnCo_2O_4$ were already crystalline as seen in Figure 21, but a post-deposition annealing was performed at 900 °C in N_2 flow in order to test the stability of the coating at higher temperatures. In order to further test the performance of $MnCo_2O_4$ coatings in the SOFC operating conditions, the samples were studied by exposure testing at 700 °C for 1000 h in air. As seen in Figure 22, the ALD coatings exhibited uniform thickness and had a dense microstructure even after the exposure test.

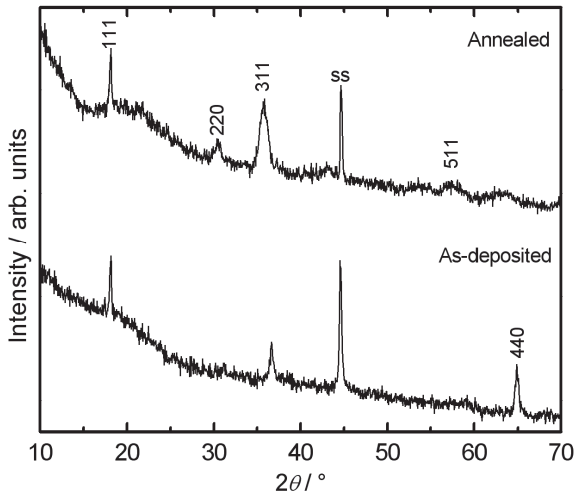

Figure 21. XRD patterns for as-deposited and post-deposition annealed (in air at 900 °C) $MnCo_2O_{4+\delta}$ films deposited on stainless steel (Crofer22 APU). The indices are for the cubic space group $Fd\bar{3}m$.

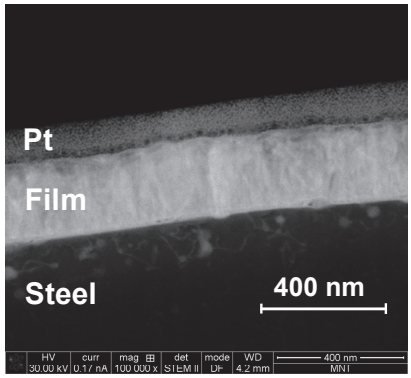

Figure 22. Cross-section micrograph (by TEM) of an ALD coating of $MnCo_2O_4$ (250 nm) on Crofer 22 APU steel tested for 1000 h in air at 700 °C.

8 CONCLUSIONS

Special synthesis conditions are often the key to finding novel functional materials. Bringing the new materials closer to their potential applications through thin-film techniques is moreover a vital step in creating materials solutions for future generations. In the present thesis, the synthesis of several ternary manganese oxides with enticing magnetic properties was realized in both powder and thin-film forms.

An entire series of the hexagonal RMnO$_3$ system was synthesized for R = Y, Ho-Lu, and then converted to orthorhombic perovskites through high-pressure treatment. A systematic study of the structural evolution showed that the lattice parameters of both polymorphs increase linearly as $r(R^{III})$ increases. The progressive reduction in the size of R^{III} increases the distortion of the *o*-RMnO$_3$ perovskites. Both the hexagonal and orthorhombic RMnO$_3$ series showed an AFM ordering of the Mn moments at low temperatures. High-quality thin-film samples of the hexagonal and orthorhombic RMnO$_3$ families were fabricated employing the ALD technique and subsequent heat treatment. The formation of metastable orthorhombic RMnO$_3$ perovskites of the small rare earths was successfully promoted even for the smallest R constituent, Lu, by depositions on coherent perovskite substrates with low lattice mismatch with the targeted structure. The magnetic properties determined for the RMnO$_3$ thin films featuring AFM-type ordering were in good accordance with the corresponding results on powder samples. The ferromagnetic interactions in the LaMnO$_{3+\delta}$ or La$_{1-x}$Mn$_{1-x}$O$_3$ films revealed the presence of cation vacancies in the structure.

Spinel-structured (Mn,Co)$_3$O$_4$ thin films were reproducibly fabricated by ALD. Precise control of the oxygen content of as-deposited MnCo$_2$O$_{4+\delta}$ films was achieved for the first time for an ALD-grown thin-film sample through post-deposition heat treatments, as evidenced from the monotonous increases of both the unit-cell volume and the Curie temperature with increasing annealing temperature/decreasing oxygen partial pressure. The application potential of ALD-grown MnCo$_2$O$_4$ films as protective coatings in solid oxide fuel cells was moreover studied with extremely promising results.

REFERENCES

1. E. Lundblad, *Kosmos* **43** (1965) 81-95.
2. H. Yamauchi, M. Karppinen, *Supercond. Sci. Technol*. **13** (2000) R33.
3. F. P. Bundy, H. T. Hall, H. M. Strong, R. H. Wenthorf Jr., *Nature* **176** (1955) 51.
4. S. Adachi, H. Yamauchi, S. Tanaka, N. Mori, *Physica C* **208** (1993) 226.
5. S. Adachi, H. Yamauchi, S. Tanaka, N. Mori, *Physica C* **212** (1993) 164.
6. O. Yu. Gorbenko, S. V. Samoilenkov, I. E. Graboy, A. R. Kaul, *Chem. Mater.* **14** (2002) 4026.
7. D. P. Norton, B. C. Chakoumakos, J. D. Budai, J. R. Thompson, D. H. Lowndes, *J. Supercond.* **8** (1995) 519.
8. A. Kaul, O. Gorbenko, M. Novojilov, A. Kamenev, A. Bosak, A. Mikhaylov, O. Boytsova, M. Kartavseva, *J. Cryst. Growth* **275** (2005) e2445.
9. C. Girardot, F. Conchon, A. Boulle, P. Chaudouet, N. Caillault, J. Kreisel, R. Guinebretière, F. Weiss, S. Pignard, *Surf. Coat. Tech.* **201** (2007) 9021.
10. S. Havelia, S. Wang, K. R. Balasubramaniam, P. A. Salvador, *J. Solid State Chem.* **182** (2009) 1603.
11. M. Putkonen, T. Sajavaara, L. Niinistö, J. Keinonen, *Anal. Bioanal. Chem.* **382** (2005) 1791.
12. S. M. George, *Chem. Rev.* **110** (2010) 111.
13. M. Ritala, J. Niinistö, *ECS Trans.* **25** (2009) 641.
14. M. Knez, K. Nielsch, L. Niinistö, *Adv. Mater.* **19** (2007) 3425.
15. E.F. Bertaut, F. Forrat, P.H. Fang, *C. R. Acad. Sci. Paris* **265** (1963) 1958.
16. H. Y. Hwang, S.-W. Cheong, P. G. Radaelli, M. Marezio, B. Batlogg, *Phys. Rev. Lett.* **75** (1995) 914.
17. R. Von Helmolt, J. Wecker, B. Holzapfel, L. Schultz, K. Samwer, *Phys. Rev. Lett.* **71 (**1993) 2331.
18. Z. J. Huang, Y. Cao, Y. Y. Sun, Y. Y. Xue, C. W. Chu, *Phys. Rev. B* **56 (**1997) 2623.

19. M. Fiebig, Th. Lottermosser, D. Fröhlich, A. V. Goltsev, R. V. Pisarev, *Nature* **419 (**2002) 818.
20. T. Kimura, T. Goto, H. Shintani, K. Ishizaka, T. Arima, Y. Tokura, *Nature* **426** (2003) 55.
21. E. Ríos, O. Peña, T. Guizouarn, J.-L. Gautier, *Pys. Sat. Sol. (C)* **1** (2004) S108.
22. G. V. Bazuev, A. V. Korolov, *J. Magn. Magn. Mater*. **320** (2008) 2262.
23. P. A. Joy, S. K. Date, *J. Magn. Magn. Mater.* **210** (2000) 31.
24. P. A. Joy, S. K. Date, *J. Magn. Magn. Mater.* **218** (2000) 229.
25. H. L. Yakel Jr. *Acta Cryst.* **8 (**1955) 394.
26. H. L. Yakel Jr., W. C. Koehler, E. F. Bertaut, F. Forrat, *Acta Cryst.* **16 (**1963) 957.
27. R. J. H. Voorhoeve, J. P. Remeika, P. E. Freeland, B. T. Matthias, *Science* **177 (**1972) 353.
28. B. Levasseur, S. Kaliaguine, *J. Solid State Chem.***181 (**2008) 2953.
29. M. J. Koponen, T. Venäläinen, M. Suvanto, K. Kallinen, T.-J. J. Kinnunen, M. Härkönen, T. A. Pakkanen, *Catal. Lett.* **111** (2006) 75.
30. (a) A. Waintal, J. J. Capponi, E. F. Bertaut, M. Contré, D. François, *Solid State Commun.*, **4** (1966) 125. (b) A. Waintal, J. Chevanas, *Mater. Res. Bull.* **2** (1967) 819.
31. Y. H. Huang, H. Fjellvåg, M. Karppinen, B. C. Hauback, H. Yamauchi, J. B. Goodenough, *Chem. Mater.* **18** (2006) 2130.
32. J.-S., Zhou, J. B. Goodenough, J. M. Gallardo-Amores, E. Morán, M. A., Alario-Franco, R. Caudillo, *Phys. Rev. B* **74** (2006) 14422.
33. G. Zhu, P. Liu, Y. Liu, H. Miao, J. Zhou, *J. Am. Chem. Soc.* **91** (2008) 3423.
34. E. S. Stampler, W. C. Sheets, W. Prellier, T. J. Marks, K. R. Popperlmeier, *J. Mater. Chem.***19** (2009) 4375.
35. P. A. Salvador, T.-D- Doan, B. Mercey, B. Raveau, *Chem. Mater.* **10** (1998) 2592.

36. A. A. Bosak, A. A. Kamenev, I. E. Graboy, S. V. Antonov, O. Yu. Gorbenko, A. R. Kaul, C. Dubourdieu, J. P. Senator, V. L. Svechnikov, H. W. Zandbergen, B. Holländer, *Thin Solid Films* **400** (2001) 149.
37. S. Quezel, J. Rossat Mignot, E. F. Bertaut, *Solid State Commun*. **14** (1974) 941.
38. H. W. Brinks, H. Fjellvåg, A. Kjekshus, *J. Solid State Chem*. **129** (1997) 334.
39. J. A. Alonso, M. J. Martínez-Lope, M. T. Casáis, M. T. Fernández-Díaz, *Inorg. Chem.* **39** (2000) 917.
40. Y. Wang, X. Lu, Y. Chen, F. Chi, S. Feng, X. Liu, *J. Solid State Chem*. **178** (2005) 1317.
41. L. Martín-Carrón, A. de Andrés, M. J. Martínez-Lope, M. T. Casais, J. A. Alonso, *Phys. Rev. B* **66** (2002) 174303.
42. J. Spooren, R. I. Walton, F. Millange, *J. Mater. Chem*. **15** (2005) 1542.
43. A.-C. Gaillot, D. Flot, V. A. Drits, A. Manceau, M. Burghammer, B. Lanson, *Chem. Mater*. **15** (2003) 4666.
44. A.-C. Gaillot, B. Lanson, V. A. Drits, *Chem. Mater*. **17** (2005) 2959.
45. N. Imamura, M. Karppinen, H. Fjellvåg, H. Yamauchi, *Solid State Commun.* **140** (2006) 386.
46. H. Okamoto, H. Fjellvåg, H. Yamauchi, M. Karppinen, *Solid State Commun.* **137** (2006) 522.
47. A. A. Bosak, C. Dubourdieu, J.-P. Sénateur, O. Yu. Gorbenko, A. R. Kaul, *J. Mater. Chem.* **12** (2002) 800.
48. J.-H. Lee, P. Murugavel, H. Ryu, D. Lee, J. Y. Jo, J. W. Kim, H. J. Kim, K. H. Kim, Y. Jo, M.-H. Jung, Y. H. Oh, Y.-W. Kim, J.-G. Yoon, J.-S. Chung, T. W. Noh, *Adv. Mater.* **18** (2006) 3125.
49. K. R. Balasubramaniam, S. Havelia, P. A. Salvador, H. Zheng, J. F. Mitchell, *Appl. Phys. Lett.* **91** (2007) 232901.
50. T. Katsufuji, M. Masaki, A. Machida, M. Moritomo, K. Kato, E. Nishibori, M. Takata, M. Sakata, K. Ohoyama, K. Kitazawa, H. Takagi, *Phys. Rev. B* **66** (2002) 134434.

51. R. D. Shannon, *Acta Cryst. A* **32** (1976) 751.
52. Y. Q. Jia, *J. Solid State Chem.* **95** (1991) 184.
53. M. Tachibana, T. Shimoyama, H. Kawaji, T. Atake, E. Takayama-Muromachi, Phys. Rev. B 75 (2007) 144425.
54. V. M. Goldschmidt, *Naturwissenschaften* **14** (1926) 477.
55. J. Rodríguez-Carvajal, M. Hennion, F. Moussa, A. H. Moudden, L. Pinsard, A. Revcolevschi, *Phys. Rev. B* **57** (1998) R3189.
56. T. Mori, N. Kamegashira, K. Aoki, T. Shishido, T. Fukuda, *Mater. Lett.* **54** (2002) 238.
57. N. A. Spaldin, M. Fiebig, *Science* **309** (2005) 391.
58. N. A. Hill, *J. Phys. Chem. B* **104** (2000) 6694.
59. Th. Lonkai, D. G. Tomuta, U. Amann, J. Ihringer, R. W. A. Hendrikx, D. M. Többens, J. A. Mydosh, J. A., *Phys. Rev. B* **69** (2004) 134108.
60. K. Yoshii, H. Abe, *J. Solid State Chem.* **165** (2002) 131.
61. T. Kimura, S. Ishihara, H. Shintani, T. Arima, K. T. Takahashi, K. Ishizaka, Y. Tokura, *Phys. Rev. B* **68** (2003) 60403.
62. R. Mahendiran, S. K. Tiwary, A. K. Raychaudhuri, T. V. Ramakrishnan, R. Mahesh, N. Rangavittal, C. N. R. Rao, *Phys. Rev. B* **53** (1996) 3348.
63. B. C. Tofield, W. R. Scott, *J. Solid State Chem.* **10** (1974) 183.
64. V. A. Cherepanov, L. Yu. Barkhatova, A. N. Petrov, V. I. Voronin, *J. Solid State Chem.* **118** (1995) 53.
65. T. Nissinen, Y. Kiros, M. Gasik, M. Lampinen, M. *Mater. Res. Bull.* **39** (2004) 1195.
66. A. Restovic, E. Ríos, S. Barbato, J. Ortiz, J. L. Gautier, *J. Electroanal. Chem.* **522** (2002) 141.
67. M. Sugawara, M. Ohno, K. Matsuki, *J. Mater. Chem.* **7** (1997) 833.
68. Q. Liang, K. Chen, W. Hou, Q. Yan, *Appl. Catal. A* **166** (1998) 191.
69. P. Umadevi, C. L. Nagendra, *Sens. Actuators A* **96** (2002) 114.

70. X. Chen, P. Y. Hou, C. P. Jacobson, S. J. Visco, L. C. D. Jonghe, *Solid State Ionics* **176** (2005) 425.
71. Y. Larring, T. Norby, *J. Electrochem. Soc.* **147** (2000) 3251.
72. Z. Yang, G. Xia, S. P. Simner, J. W. Stevenson, *Electrochem. Soc.* **152** (2005) A1896.
73. D. G. Wickham, W. J. Croft, *Phys. Chem. Solids* **7** (1958) 351.
74. G. Blasse, *Philips Res. Rep.* **18** (1963) 383.
75. E. F. Vainshtein, R. M. Ovrutskaya, B. I. Kotlyar, *Sov. Phys. Solid State* **7** (1966) 1707.
76. Y. T. Chong, E. M. Y. Yau, K. Nielsch, J. Bachmann, *Chem. Mater.* **22** (2010) 6506.
77. S. W. Lee, J. H. Han, S. Han, W. Lee, J. H. Jang, M. Seo, S. K. Kim, C. Dussarrat, J. Gatineau, Y.-S. Min, C. S. Hwang, *Chem. Mater.* **23** (2011) 2227.
78. V. Pore, M. Dimri, H. Khanduri, R. Stern, J. Lu, L. Hultman, K. Kukli, M. Ritala, M. Leskelä, *Thin Solid Films* **519** (2011) 3318.
79. O. Nilsen, E. Rauwal, H. Fjellvåg, A. Kjekshus, *J. Mater. Chem.* **17** (2007) 1466.
80. M. Nieminen, T. Sajavaara, E. Rauhala, M. Putkonen, L. Niinistö, *J. Mater. Chem.* **11** (2001) 2340.
81. P. Myllymäki, M. Nieminen, J. Niinistö, M. Putkonen, K. Kukli, L. Niinistö, *J. Mater. Chem.* **16** (2006) 563.
82. T. P. Holme, C. Lee, F. B. Prinz, *Solid State Ionics* **179** (2008) 1540.
83. T. Aaltonen, M. Alnes, O. Nilsen, L. Costelle, H. Fjellvåg, *J. Mater. Chem.* **20** (2010) 2877.
84. P. Myllymäki, M. Roeckerath, J. M. Lopes, J. Schubert, K. Mizohata, M. Putkonen, L. Niinistö, *J. Mater. Chem.* **20** (2010) 4207.
85. J. Päiväsaari, M. Putkonen, L. Niinistö, *Thin Solid Films* **472** (2005) 275.
86. M. Nieminen, M. Putkonen, L. Niinistö, *Appl. Surf. Sci.* **174** (2001) 155.

87. K. Binnemans, In: *Handbook on the Physics and Chemistry of Rare Earths*, Vol. **35** (Eds. K. A. Gscneider Jr., J.-C. G. Bünzli, V. K. Percharsky), Elsevier, Amsterdam 2005, pp. 107.
88. L. I. Martynenko, N. P. Kuz'mina, A. N. Grigor'ev, *Russ. J. Inorg. Chem.*, **43** (1998) 1038.
89. J. P. R. De Villiers, J. C. A. Boyens, *Acta Cryst. B*, **27** (1971) 2335.
90. M. Lie, K. B. Klepper, O. Nilsen, H. Fjellvåg, A. Kjekshus, *Dalton Trans.* **2008** 253.
91. K. B. Klepper, O. Nilsen, H. Fjellvåg, *Thin Solid Films* **515** (2007) 7772.
92. K. B. Klepper, O. Nilsen, H. Fjellvåg, *J. Cryst. Growth* **307** (2007) 457.
93. O. Nilsen, H. Fjellvåg, A. Kjekshus, *Thin Solid Films* **444** (2003) 44.
94. S. T. Oyama, *Catal. Rev.-Sci. Eng.* **42** (2000) 279
95. N. Adachi, V. P. Denysenkov, S. I. Khartsev, A. M. Grishin, T. Okuda, *J. Appl. Phys.* **88** (2000) 2734.
96. A. A. Bosak, O. Yu, Gorbenko, A. R. Kaul, I. E. Graboy, C. Dubordieu, J. P. Senateur, H. W. Zandbergen, *J. Magn. Magn. Mater.* **211** (2000) 61.
97. T. Heeg, M. Roeckerath, J. Schubert, W. Zander, C. Buchal, H. Y. Chen, C. L. Jia, Y. Jia, C. Adamo, D. G. Schlom, *Appl. Phys. Lett.* **90** (2007) 192901.
98. L. J. LeGore, O. D. Greenwood, J. W. Paulus, D. J. Frankel, R. J. Lad, *J. Vac. Sci. Technol. A* **15** (1997) 1223.
99. T. Fujii, M. Takano, R. Katano, Y, Bando, Y. Isozumi, *J. Appl. Phys.* **66** (1989) 3168.
100. F. C. Voogt, T. Fujii, P. J. M. Smulders, L. Niesen, M. A. James, T. Hibma, *Phys. Rev. B* **60** (1999) 11193.
101. P. Lacorre, J. B. Torrance, J. Pannetier, A. I. Nazzal, P. W. Wang, T. C. Huang, *J. Solid State Chem* **91** (1991) 225.
102. M. A. Novojilov, O. Yu. Gorbenko, I. E. Graboy, A. R. Kaul, H. W. Zandbergen, N. A. Babuchkina, L. M. Belova, *Appl. Phys. Lett.* **76** (2000) 2041.

103. J. Harjuoja, S. Väyrynen, M. Putkonen, L. Niinistö, E. Rauhala, *J. Cryst. Growth* **286** (2006) 376.

104. J. Harjuoja, S. Väyrynen, M. Putkonen, L. Niinistö, E. Rauhala, *Appl. Surf. Sci.* **253** (2007) 5228.

105. H. Wang, J.-J. Wang, R. Gordon, J.-S. M. Lehn, H. Li, D. Hong, D. V. Shenai, *Electrochem. Solid-State Lett.* **12** (2009) G13.

106. J.-S. Zhou, J. B. Goodenough, *Phys. Rev. B* **68** (2003) 054403.

107. D. N. Argyriou, N. Aliouane, J. Strempfer, I. Zegkinoglou, B. Bohnenbuck, K. Habicht, M. v. Zimmermann, *Phys. Rev. B* **75** (2007) 020101.

108. J. Töpfer, J. B. Goodenough, *J. Solid State Chem.* **130** (1997) 117.

109. J. A. Alonso, M. J. Martínez-Lope, M. T. Casais, J. L. MacManus-Driscoll, P. S. I. P. N. de Silva, L. F. Cohen, M. T. Fernández-Díaz, *J. Mater. Chem.* **7** (1997) 2139.

110. F. M. M. Borges, D. M. A. Melo, M. S. A. Camara, A. E. Martinelli, J. M. Soares, J. H. de Araújo, F. A. O. Cabral, *J. Magn. Magn. Mater.* **302** (2006) 273.

111. T. Kadowaki, T. Shiomitsu, E. Matsuda, H. Nakagawa, H. Tsuneisumi, *Solid State Ionics* **67** (1993) 65.

112. S. Linderoth, *Surf. & Coating Tech.*, **80** (1996) 185.

113. W. J. Quadakkers, H. Greiner, M. Hänsel, A. Pattanaik, A. S. Khanna, W. Malléner, *Solid State Ionics* **91** (1996) 55.

114. J.-H. Kim, R.-H. Song, S.-H. Hyun, *Solid State Ionics* **174** (2004) 185.

115. Z. Yang, G.-G. Xia, G. D. Maupin, J. W. Stevenson, *J. Electrochem. Soc.* **153** (2006) A1852.

116. Z. Yang, K. S. Weil, D. M. Paxton, J. W. Stevensson, *J. Electrochem. Soc.* **150** (2003) A1188.

117. Z. Yang, J. S. Hardy, M. S. Walker, G. Xia, S. P. Simner, J. W. Stevenson, *J. Electrochem. Soc.* **151** (2004) A1825.

118. T. Horita, H. Kishimoto, K. Yamaji, Y. Xiong, N. Sakai, M. E. Brito, H. Yokokawa, *J. Electrochem. Soc.* **153** (2006) A2007.

119. Z. Yang, J. W. Stevensson, P. Singh, in *Materials for the Hydrogen Economy*, ed. R. H. Jones, G. J. Thomas, CRC Press, Boca Raton, FL, vol. 1, pp. 229.
120. K. Hilpert, D. Das, M. Miller, D. H. peck, R. Weiss, *J. Electrochem. Soc.* **143** (1996) 3642.
121. C. C. Mardare, H. Asteman, M. Spiegel, A. Savan, A. Ludwig, *Appl. Surf. Sci*, **255** (2008) 1850.
122. J.-J. Choi, J. Ryu, B.-D- Hahn, W.-H. Yoon, B.-K. Lee, D.-S. Park, *J. Mater. Sci.* **44** (2009) 843.

The search for new functional materials is a fascinating task filled with challenges. It is also a vital step in the development of many future applications, e.g. among data storage or novel energy solutions, whose functionality relies on the innovations made in the field of materials science. In order to extend the selection of materials, methods employing special synthesis conditions are often needed, as they offer powerful tools for designing sophisticated solutions. This thesis reports the synthesis and characterization of ternary manganese oxide materials featuring interesting magnetic properties. The synthesis through several techniques, the characterization of structural and magnetic properties, and the possibility to alter the oxygen stoichiometry of thin films are presented. The thesis provides important additions to the selection of magnetic materials fabricated through atomic layer deposition (ALD), and includes the first study on the control of oxygen stoichiometry of ALD-grown thin films.

ISBN 978-952-60-4178-0 (pdf)
ISBN 978-952-60-4177-3
ISSN-L 1799-4934
ISSN 1799-4942 (pdf)
ISSN 1799-4934

Aalto University
School of Chemical Technology
Department of Chemistry
www.aalto.fi

BUSINESS + ECONOMY

ART + DESIGN + ARCHITECTURE

SCIENCE + TECHNOLOGY

CROSSOVER

DOCTORAL DISSERTATIONS

Aalto-DD 56/2011